HELSINKI INSTITUTE OF PHYSICS INTERNAL REPORT SERIES

HIP-2021-02

Non-Perturbative Approach to the Electroweak Phase Transition in Extended Higgs Sectors

Lauri Niemi

Helsinki Institute of Physics
University of Helsinki
Finland

DOCTORAL DISSERTATION

To be presented for public discussion with the permission of the Faculty of Science of the University of Helsinki, in Auditorium A111, Exactum building, on the 28th of September, 2021 at 15 o'clock.

Helsinki 2021

ISBN 978-951-51-1297-2 (print)
ISBN 978-951-51-1298-9 (pdf)
ISSN 1455-0563
http://ethesis.helsinki.fi
Unigrafia
Helsinki 2021

L. Niemi: Non-Perturbative Approach to the Electroweak Phase Transition in Extended Higgs Sectors,
University of Helsinki, 2021, 65 pages,
Helsinki Institute of Physics, Internal Report Series, HIP-2021-02,
ISBN 978-951-51-1297-2,
ISSN 1455-0563.

Abstract

Many candidate theories for physics beyond the Standard Model predict that the early universe could have undergone first-order phase transitions. In particular, if new physics exists near the electroweak scale, the phase transition associated with the electroweak Higgs mechanism could have been first order. Such electroweak phase transition would be particularly interesting for cosmology, as it could provide the necessary conditions for baryogenesis and act as a source of gravitational radiation that could be detected in forthcoming gravitational-wave experiments.

The purpose of this thesis is to build a robust understanding of the thermodynamics associated with cosmological phase transitions in particle physics models involving new scalars. While the zero-temperature behavior of such theories is often well described by perturbation theory, at finite temperatures this methodology breaks down due to severe infrared divergences at temperatures close to the phase transition point, making it impossible to reliably probe the order and other properties of the transition within perturbation theory alone. While estimates for characteristic quantities such as the critical temperature and latent heat can be obtained with perturbative methods, such predictions are typically sensitive to higher-order corrections from light bosons, and ultimately a non-perturbative solution to the problem is required. The framework discussed in the thesis avoids these issues by simulating the problematic long-distance physics non-perturbatively on the lattice, allowing for a rigorous determination of the thermodynamical parameters that are crucial for making cosmologically interesting predictions related to gravitational waves and baryogenesis.

The thesis presents a theoretical review of the electroweak phase transition and associated non-perturbative effects and proceeds then to study a selection of popular scalar extensions of the Standard Model. Strong first-order phase transitions are found also at the non-perturbative level, but their quantitative properties differ substantially from the leading-order perturbative predictions. We demonstrate in typical strong-transition scenarios that while the perturbative method is significantly more accurate once the calculation is extended to the 2-loop level, there remains a discrepancy of order 10% for the critical temperature and several tens of percents for the latent heat, relative to the non-perturbative results. Based on our results, the 2-loop improvement should be considered essential for even order-of-magnitude estimates of the thermodynamical parameter, and these predictions will likely need non-perturbative verification if accurate results are needed.

Acknowledgements

I thank my supervisors Kari Rummukainen, David Weir and Venus Keus for their continuous support and guidance over the years. I have learned a lot from our mutual projects, and I am deeply grateful for your patience during the times when my barrage of questions probably seemed endless. I also thank the pre-examiners of this thesis, professors Arttu Rajantie and York Schröder, for carefully reading through the initial manuscript, and professor Mikhail Shaposhnikov for agreeing to be my opponent.

During my studies I had the pleasure to visit several universities around the world. In particular, I thank professor Mikko Laine for the opportunity to visit Bern, and professor Michael Ramsey-Musolf for his hospitality in both Amherst and Shanghai. I am also grateful to my supervisors for sending me to fascinating conferences and schools.

The research leading up to this thesis has been a collaborative effort, for which I am indebted to my collaborators: Oliver Gould, Kimmo Kainulainen, Michael Ramsey-Musolf, Philipp Schicho, Tuomas Tenkanen, Ville Vaskonen, and of course my supervisors. I also thank all the postdocs and fellow students in the computational field theory group for fruitful coffee-break discussions and social events over the years. Special thanks to David, Tuomas and Kalle Ala-Mattinen for the mutual time spent at various conferences, and to professor Aleksi Vuorinen for support that has continued since early days of my master's studies.

I acknowledge financial support from the Jenny and Antti Wihuri foundation. The numerical simulations for this research were carried out on supercomputers at the CSC in Espoo, Finland, and on the University of Helsinki cluster Kale.

Finally, I wish to express my gratitude to my family and friends for their persistent support, and especially to Sandra for the delightful time we have spent together and for convincing me that life exists outside of physics as well.

Included publications

The thesis is based on the following publications [1–3]:

I On the validity of perturbative studies of the electroweak phase transition in the Two Higgs Doublet model
K. Kainulainen, V. Keus, L. Niemi, K. Rummukainen, T. V. I. Tenkanen and V. Vaskonen
JHEP 06, 075 (2019)

II Thermodynamics of a two-step electroweak phase transition
L. Niemi, M. J. Ramsey-Musolf, T. V. I. Tenkanen and D. J. Weir
Phys. Rev. Lett. 126, 171802 (2021)

III Singlet-assisted electroweak phase transition at two loops
L. Niemi, P. Schicho and T. V. I. Tenkanen
Phys. Rev. D. 103, 115035 (2021)

The authors are listed in alphabetical order in accordance with the particle physics convention.

The author's contributions

For papers I and II, the author carried out all simulations and performed their numerical analysis. The author also participated in the 2-loop perturbative calculations. For paper III the author calculated the effective potential in parallel with the collaborators and carried out the numerical analysis.

For all publications I-III the initial manuscripts were drafted by the author and expanded on by the collaborators.

Contents

Chapter 1

Introduction

A recurring theme across various areas of physics is that when a macroscopic number of small constituents of matter – particles – are brought together, they can exhibit collective phenomena that bear no immediate resemblance to the behavior of individual, isolated particles. A striking example is provided by phase transitions, where the macroscopic behavior of the system changes rapidly, possibly even discontinuously as in a first-order phase transition. Phase transitions can be triggered by a change in some external parameter, such as the temperature.

The microscopic behavior of matter is described by quantum field theories (QFTs), and currently the best theory of all known particles is a particular QFT known as the Standard Model (SM) of particle physics. With the discovery of its last ingredient, the Higgs boson, in 2012 [4, 5], the SM is a complete framework with no unknown parameters left. Feeling adventurous, we may ask: How does the matter content of the SM behave when exposed to extreme temperatures, and does the theory undergo phase transitions as the temperature is varied?

There are two obvious temperature ranges where we may expect interesting physics to arise: In the Quantum Chromodynamics (QCD) sector at temperature $T_{\mathrm{QCD}} \sim 100$ MeV, associated with the transition between quark-gluon plasma and hadronic matter, and in the electroweak (EW) sector around $T_{\mathrm{EW}} \sim 100$ GeV in connection with the EW Higgs mechanism. Standard cosmology predicts that such temperatures were prevalent at very early times, as the expanding universe cooled down from a hot initial state in the aftermath of cosmic inflation. Thus the question of phase transitions within the SM is more than a curious thought experiment; it is deeply intertwined with early-universe cosmology.

By now, the phase structure of hot SM is well established. There is, in fact, no finite-T phase transition of *any* order in QCD [6] nor in the EW sector [7, 8].[1] Instead, in both cases the universe would smoothly interpolate between the low- and high-temperature regimes in a behavior called *crossover*. But it is also known that the SM cannot be the final theory of the universe. Indeed, some of the most obvious indicators are the absence of a dark matter candidate and the the lack of antimatter in the universe, for which the SM provides no explanation. Since it is extremely likely that new matter content needs to be introduced as solutions to these problems, there is

[1] QCD is known to admit a rich phase diagram with first-order transitions at large baryon chemical potentials [9], but these are extremely small in the early universe and play little role in cosmological phase transitions.

motivation to investigate how the finite-T phase structure may be affected by new fields in the theory.

This thesis discusses the possibility of having a first-order phase transition around the EW scale. Such phase transition would have a number of interesting consequences. First is the mechanism of electroweak baryogenesis (EWBG) [10–12], which provides a plausible explanation for why the universe contains substantially more matter than antimatter [13]. The general conditions for any baryogenesis scenario were identified by Sakharov [14] and are (i) baryon number non-conservation, (ii) C and CP violation, and (iii) deviations from thermal equilibrium. The SM fails to fulfill (iii), as it predicts only smooth crossovers in the early universe. The condition (i) is satisfied at finite temperature by non-perturbative sphaleron transitions that violate the baryon number through the axial anomaly [15, 16]. C violation appears naturally in the chirally-coupled EW theory, and CP is violated by Yukawa interactions in the SM.

A first-order electroweak phase transition (EWPT) proceeds through nucleation of expanding bubbles of the low-T phase, where the Higgs mechanism is active and the rate of sphaleron transitions is exponentially suppressed. In the EWBG scenario, CP-violating scatterings in the vicinity of bubble walls bias unsuppressed sphalerons to generate a baryonic excess, which gets swept inside the bubble and is preserved, provided the sphaleron suppression is strong enough. Semiclassically, this requires that the Higgs vacuum-expectation value, which jumps discontinuously across the bubble wall, satisfies $v \gtrsim T$ immediately after the transition. This is the baryogenesis criterion for a *strong* EWPT. Realistic models of EWBG should also include additional CP-violating sources, as the amount of CP violation within the SM alone appears inadequate [17–19]. Reviews of EWBG can be found in [20–22].

Another important consequence is the production of gravitational waves during the phase transition. First-order phase transitions are characterized by a discontinuity in the total energy density. Once bubbles of the low-T phase nucleate in the early universe, most of the released energy is absorbed by the surrounding primordial plasma or spent in the formation of the bubble walls. Gravitational waves are produced towards the end of the transition, when bubbles formed in different regions of space collide and eventually fill the entire universe with the new phase [23, 24]. The collisions create an anisotropic environment where gravitational radiation is sourced by shear-stress components of the energy-momentum tensor [25, 26]. Modeling the macroscopic bubble dynamics with relativistic fluid equations, numerical simulations have revealed that the dominant gravitational-wave signal arises from long-lived sound waves in the cosmic plasma after the bubble collisions [27–30].

The waves interact only weakly with matter and would survive in the present universe as a stochastic gravitational-wave background. Remarkably, the power spectrum of gravitational waves from a first-order transition around the EW temperature would be peaked in the millihertz range, which is within the sensitivity window of the upcoming LISA experiment [31, 32]. Thus if a first-order EWPT occurred in the early universe, there are promising prospects for detecting gravitational relics from it in the near future, in LISA or in other detectors [33–35]. An observation of such gravitational waves could also be an indirect sign of new physics, acting as a complementary probe to particle accelerator experiments. Of particular interest also for gravitational-wave production are strong phase transitions, and the appropriate measure in this context is the latent

heat[2] [36].

Quite intuitively, achieving a strong EWPT requires drastic modifications to the Higgs potential as the minimal SM does not have even a first-order transition, yet alone a strong one. The simplest way of turning the EW crossover into a first-order transition is to couple the Higgs to new scalar fields. It is also intuitively clear that if the resulting beyond the SM (BSM) theory features a strong EWPT, the new particles responsible for it cannot be exceedingly heavier than the SM Higgs and could therefore be probed directly in particle accelerators [37, 38]. Indeed, ongoing and planned collider experiments [39–42] will thoroughly explore the structure of the Higgs sector, and many candidate theories featuring first-order EWPT are likely to face considerable restrictions (or in the fortunate case, confirmation) on their allowed particle content. Thus the EWPT scenario is a testable one, and tightly connected with the phenomenology of BSM models.

Should a stochastic gravitational-wave signal be detected, it becomes important to investigate whether it originates from a cosmological first-order phase transition, or from some other stochastic source in the early universe [43]. In particular, we may ask whether a specific BSM scenario can explain the observed signal, and investigating this requires reliable methods for computing the gravitational-wave spectrum starting from underlying particle physics. For first-order transitions specifically, this requires a thorough understanding of the associated thermodynamics (critical temperature and latent heat) and the real-time rate of bubble nucleation, which act as inputs for the fluid simulations [27–30]. Essentially the same computations are pre-requisites for understanding prospects for baryogenesis in a given BSM model. Thus there is a clear demand for robust predictions about the finite-T behavior of these models.

The purpose of this thesis is to describe a *non-perturbative* framework for studying the EWPT in BSM scenarios involving additional scalar fields. This approach may seem strange at first, because the standard EW theory in the vacuum is weakly coupled and described perfectly well by perturbative methods. This, however, does not carry over to finite temperature, where perturbation theory breaks down at long distances due to high occupation numbers of bosons [44, 45]. The problem is most severe precisely near the EWPT temperature, and it is not obvious how accurate perturbative predictions of *e.g.* the transition strength are. Most phenomenological studies of the EWPT in BSM settings are based on the 1-loop effective potential: a far from exhaustive list of references is [46–79]. Yet, extended studies demonstrate that the results can be very sensitive to higher-order corrections [1–3, 80–84]. For instance, ref. [84] shows several orders of magnitude uncertainty in the peak gravitational-wave amplitude, arising from residual renormalization-scale dependence alone. Already establishing the order of the EWPT is, strictly speaking, beyond the reach of perturbation theory, and it is only because of non-perturbative lattice simulations that the SM crossover behavior is now understood [7, 8, 85–88]. The methods discussed in this thesis are aimed at building a robust understanding of the finite-T behavior of BSM theories, both through higher-order perturbative calculations but ultimately at the non-perturbative level using lattice simulations.

More specifically, our approach is a combination of finite-T perturbation theory for degrees of freedom for which it is reliable, and non-perturbative simulations for the strongly-coupled

[2] A more general specification of the phase transition strength, as relevant for gravitational-wave production, can be given in terms of the trace anomaly [30].

infrared (IR) modes. This separation is achieved by working in the dimensional reduction approximation at high temperature [89, 90], which isolates the problematic long-distance physics into an effective three-dimensional (3d) theory and allows for very efficient lattice simulations of the thermodynamics. The methodology was developed and applied to the SM in [91–93]. Here we review the theoretical premise of these studies, and discuss some recent results obtained in various BSM models [1–3, 94–97].

The outline of this thesis is as follows. We begin by reviewing the basic setting of finite-temperature QFT in chapter 2, introducing also the framework of high-T dimensional reduction and discuss why thermal perturbation theory fails in the presence of long-wavelength bosons. Chapter 3 focuses on Euclidean gauge theory and discusses in particular the high-T behavior of non-abelian gauge fields. This chapter also introduces the lattice formulation of gauge theory, setting the stage for non-perturbative investigations in later chapters. Chapter 4 is a theory-driven review of the finite-T phase structure of the standard EW theory, and is a pre-requisite for understanding the EWPT at the non-perturbative level also in simple extensions of the SM. In chapter 5 we turn out attention to BSM theories, discuss the perturbative approach to the EWPT in a singlet-extended model and point out uncertainties associated with the loop expansion. As a solution to these problems, lattice Monte Carlo simulations are discussed in chapter 6, and chapter 7 applies these methods to selected BSM models. The final chapter 8 is a brief summary of the thesis.

Conventions. Thorough the thesis we will use the natural high-energy physics units, setting $c = \hbar = k_B = 1$. Unless specified otherwise, we work in Euclidean spacetime and summation of repeated indices is assumed using the Euclidean metric.

Chapter 2

Quantum field theory at finite temperature

Describing a QFT at non-vanishing temperature necessitates that in addition to the usual quantum fluctuations of the vacuum, we account for thermal fluctuations induced by interactions with the thermal medium. Properties of the system are captured by its correlation functions, or *ensemble averages*. We will work in the canonical ensemble, *i.e.* the system is taken to be in a heat bath of temperature T. It follows that the Boltzmann weight $e^{-\beta H}$, where $\beta = 1/T$, takes on the role of a density operator, and the ensemble average of a generic operator O is obtained as

$$\langle O \rangle = \frac{1}{Z} \operatorname{Tr} O e^{-\beta H}. \tag{2.1}$$

Here H is the Hamiltonian operator of the system. The normalization factor is the canonical partition function

$$Z = \operatorname{Tr} e^{-\beta H}. \tag{2.2}$$

In statistical physics, the primary quantity of interest is the free energy, which incorporates the competition between energy and entropy in the system. It is obtained from the partition function as

$$F = -T \ln Z. \tag{2.3}$$

More specifically, in the canonical ensemble this equation defines the Helmholtz free energy. In general, a phase transition occurs if the free energy is non-analytic at some temperature, and in a first-order transition the derivative $\partial F/\partial T$ is discontinuous. Here we review the formalism for calculating the free energy in the field-theoretical context.

2.1 Imaginary time formalism

Mathematically, the Boltzmann factor has the form of a quantum mechanical time-evolution operator over an *imaginary* time interval of length $1/T$. Indeed, for time-independent Hamiltonians

the time-evolution operator $U(t, t_0) = e^{-iH(t-t_0)}$ can be analytically continued to the imaginary axis by means of a *Wick rotation*, $t \to \tau = it$, to obtain

$$U(-i\tau, -i\tau_0) = e^{-(\tau-\tau_0)H} = e^{-\beta H}, \tag{2.4}$$

where we made the identification $\tau - \tau_0 = \beta$. The Wick rotation corresponds to moving from Minkowskian signature to a Euclidean one. The formulation of thermal field theory based on analytic continuation of the time coordinate is called *imaginary time formalism*. It will form the basis for our discussion of thermodynamics of the SM and its extensions.

The analogue between time evolution and the canonical density operator gives rise to specific boundary conditions for quantum fields in the imaginary time τ. Consider the two-point correlation of a Heisenberg-picture operator $\mathcal{O}$ between two points in Minkowski spacetime:[3]

$$\begin{aligned}
\langle \mathcal{O}(\mathbf{x}, t)\mathcal{O}(\mathbf{y}, t_0)\rangle =& Z^{-1}\,\mathrm{Tr}\left[\mathcal{O}(\mathbf{x}, t)\mathcal{O}(\mathbf{y}, t_0)e^{-\beta H}\right] \\
=& Z^{-1}\,\mathrm{Tr}\left[\mathcal{O}(\mathbf{x}, t)e^{-\beta H}e^{\beta H}\mathcal{O}(\mathbf{y}, t_0)e^{-\beta H}\right] \\
=& Z^{-1}\,\mathrm{Tr}\left[\mathcal{O}(\mathbf{x}, t)e^{-\beta H}e^{i(-i\beta H)}\mathcal{O}(\mathbf{y}, t_0)e^{-i(-i\beta H)}\right] \\
=& Z^{-1}\,\mathrm{Tr}\left[\mathcal{O}(\mathbf{x}, t)e^{-\beta H}\mathcal{O}(\mathbf{y}, t_0 - i\beta)\right] \\
=& \langle \mathcal{O}(\mathbf{y}, t_0 - i\beta)\mathcal{O}(\mathbf{x}, t)\rangle,
\end{aligned} \tag{2.5}$$

where the last equation follows from cyclicity of the trace. This is the Kubo-Martin-Schwinger (KMS) relation. In particular, if $\mathcal{O}$ is a bosonic (fermionic) field operator satisfying canonical (anti-)commutation relations, the KMS relation implies that at thermal equilibrium the field is (anti-)periodic in the imaginary time, with a period of $\beta = 1/T$. Equilibrium QFT can therefore be understood as an Euclidean field theory where one dimension is compactified on a circle of circumference $1/T$.

The Euclidean formulation makes explicit the fact that Lorentz symmetry is absent in thermal field theory, because the system is now studied in the rest frame of an external heat bath. But field theories are generally easier to formulate using Lorentz-invariant Lagrangians and associated path integrals, rather than in terms of Hamiltonians, and this is also the case for thermal field theory. The above discussion already points towards a recipe for obtaining the statistical partition function from a Minkowskian generating functional: we Wick rotate to imaginary time $\tau \in [0, \beta]$ and restrict the functional integration to field configurations that are (anti-)periodic in τ. For example, the action of a real scalar field is rotated as

$$\begin{aligned}
\int d^4x\, \mathcal{L} =& \int d^4x \left[\frac{1}{2}(\partial_t\phi)^2 - \frac{1}{2}(\partial_i\phi)^2 - V(\phi)\right] \\
\xrightarrow{t\to -i\tau}& -i\int_0^\beta d\tau \int d^3x \left[-\frac{1}{2}(\partial_\tau\phi)^2 - \frac{1}{2}(\partial_i\phi)^2 - V(\phi)\right] \equiv i\int_0^\beta d\tau \int d^3x\, \mathcal{L}_E,
\end{aligned} \tag{2.6}$$

[3]The Minkowski metric is taken to be $g_{\mu\nu} = \mathrm{diag}(+1, -1, -1, -1)$. It will play no role in later sections.

where we defined the Lagrangian in Euclidean signature as $\mathcal{L}_E = -\mathcal{L}(t \to -i\tau)$. The generating functional of zero-temperature QFT turns into

$$Z = \int\limits_{\phi(\mathbf{x},\beta)=\phi(\mathbf{x},0)} \mathcal{D}\phi(\mathbf{x},\tau)\ \exp[-\int_0^\beta d\tau \int d^3x\ \mathcal{L}_E]. \tag{2.7}$$

As the notation suggests, this expression is in fact equal to the canonical partition function (2.2). This can be verified by expanding the trace in eq. (2.2) in terms of $\langle\phi|\, e^{-\beta H}\, |\phi\rangle$ and writing the matrix elements in a path integral form, see for instance [98, 99]. Thus all finite-temperature correlation functions can be generated from the partition function by differentiating with respect to an external source term, just like at zero-temperature.

A similar exercise shows that the analogy between the thermal partition function and Wick-rotated QFT holds also in theories with more complicated field content. We point out a few subtleties related to gauge and fermion fields:

- Time components of gauge fields are Wick rotated as $A_t \to iA_\tau$ to preserve the structure of covariant derivatives, $D_t \to iD_\tau$.
- It is useful to introduce Euclidean counterparts of the Dirac matrices, γ^μ, through $\gamma_0^E = \gamma^0$ and $\gamma_k^E = -i\gamma^k$ for $k = 1, 2, 3$. The γ_μ^E are Hermitian and satisfy $\{\gamma_\mu^E, \gamma_\nu^E\} = 2\delta_{\mu\nu}$. The Wick-rotated Lagrangian of a free Dirac field reads $\mathcal{L}_E = \bar{\psi}[\gamma_\mu^E\ \partial_\mu + m]\psi$, where $\bar{\psi} = \psi^\dagger\gamma_0^E$. Fermion fields are anti-periodic in the imaginary time.
- If the theory is gauge fixed using the Faddeev-Popov procedure, the resulting ghost fields satisfy periodic boundary conditions at finite temperature, despite their Grassmannian nature. This is because they originate from a functional determinant composed of bosonic fields.

From this point on, we will consistently work in Euclidean spacetime and will drop the sub- and superscripts from Euclidean quantities. We also denote $A_\tau \equiv A_0, D_\tau \equiv D_0$.

For perturbation theory it is convenient to transform the fields into momentum space. Because of the (anti-)periodic boundary conditions at finite T, the spectrum of Fourier modes in the imaginary time direction is discrete. The momentum-space decomposition is written as

$$\phi(\tau, \mathbf{x}) = T\sum_n \int \frac{d^3p}{(2\pi)^3}\phi(\omega_n, \mathbf{p})e^{i\omega_n\tau}e^{-ix_ip_i}, \tag{2.8}$$

where the *Matsubara frequency* is $\omega_n = 2\pi nT$ for bosons and $\omega_n = (2n+1)\pi T$ for fermions, and Euclidean four-momenta will be denoted by capital letters, *e.g.* $P = (\omega_n, \mathbf{p})$. Feynman rules of perturbation theory are derived in analogy to zero-temperature QFT, for instance the free propagator $\langle\phi(K)\phi(P)\rangle_0$ for the scalar field theory in eq. (2.7) comes with a δ-function that enforces $K = -P$, and

$$\langle\phi(-P)\phi(P)\rangle_0 = \frac{1}{P^2 + m^2}. \tag{2.9}$$

As is explicit in the decomposition (2.8), loop integrals turn into *sum-integrals* at finite temperature. We introduce the following shorthand notation for integrations:

$$\int_p \equiv \left(\frac{\bar{\mu}^2 e^{\gamma_E}}{4\pi}\right)^{\epsilon} \int \frac{d^d p}{(2\pi)^d} \tag{2.10}$$

$$\sum\!\!\!\!\!\!\int_P \equiv T \sum_{n=-\infty}^{\infty} \int_p \qquad \text{(bosonic } \omega_n\text{)} \tag{2.11}$$

$$\sum\!\!\!\!\!\!\int_{\{P\}} \equiv T \sum_{n=-\infty}^{\infty} \int_p \qquad \text{(fermionic } \omega_n\text{)}, \tag{2.12}$$

where $d = 3 - 2\epsilon$ will be used for dimensional regularization and $\bar{\mu}$ is the associated renormalization scale in the $\overline{\text{MS}}$ scheme. Remarkably, the introduction of non-zero temperature has no effect on ultraviolet (UV) renormalization of the theory [98, 99]. This is because any sum-integral can be decomposed into $T = 0$ and $T \neq 0$ parts, and the finite-T contribution is suppressed by a Boltzmann factor $e^{-E/T}$.

2.2 Dimensional reduction at high temperature

The bosonic Matsubara mode with $n = 0$, the *zero mode*, plays a special role in thermal field theory. The zero modes carry no momentum in the imaginary time direction and thus their dynamics is effectively three dimensional. The modes with non-vanishing Matsubara frequency ω_n, including all fermionic modes, correspond to fluctuations of the field at shorter wavelengths than the zero mode. This interpretation is evident in the propagator (2.9), where the P_0 component suppresses propagation of non-zero modes by a term $\omega_n^2 \sim (\pi T)^2$. The modes with $\omega_n \gtrsim \pi T$ are called *hard* modes. The hierarchy between the zero- and non-zero Matsubara modes leads to an effective description of high-T equilibrium phenomena in terms of a 3d Euclidean field theory: we say the high-T theory undergoes *dimensional reduction* [89, 90]. This has important applications for the study of phase transitions.

The setup of high-T dimensional reduction is similar to Kaluza-Klein reduction of compactified field theories. In the limit $T \to \infty$, the periodic imaginary time dimension shrinks to a point and the momentum of all non-zero Matsubara modes becomes formally infinite. Thus the dynamics of these modes decouple from long-distance physics; in particular, static equilibrium properties of the theory can be described using the 3d Matsubara zero modes only (although there is a caveat, discussed below). In reality we work at a finite, instead of infinite, temperature, but this picture is still useful if T is much larger than all other mass scales in the theory. Specifically, if the zero-mode mass is $m \ll \pi T$ and the theory is perturbative at the scale πT, we may integrate out loops involving $\omega_n \neq 0$ modes by absorbing their effects into T-dependent counterterms in the zero-mode sector.[4] In particular, *all fermions get integrated out* as the fermionic ω_n is always non-vanishing.

[4]From now on, when referring to the high-T limit we mean that all zero modes have $m \ll \pi T$.

Let us see how this works in practice. Consider a "toy" scalar theory in dimensional regularization,

$$S = \int_0^{1/T} d\tau \int d^d x \, \left[\frac{1}{2}(\partial_\mu \phi)^2 + \frac{1}{2} m^2 \phi^2 + \frac{1}{4!}\lambda \phi^4 + \mathcal{L}_{\rm ct} \right], \tag{2.13}$$

where $\mathcal{L}_{\rm ct}$ contains UV counterterms as required to render the theory finite. At high temperatures, we can integrate over the hard modes to obtain a 3d effective field theory (EFT) with the same symmetries as (2.13):

$$S^{(3{\rm d})} = \frac{1}{T} \int d^d x \, \left[c_0(T) + \frac{1}{2} Z_\phi (\partial_\mu \phi)^2 + \frac{1}{2} \bar{m}^2 Z_\phi \phi^2 + \frac{1}{4!} \bar{\lambda} Z_\phi^2 \phi^4 + \mathcal{L}_{\rm ct}^{(3{\rm d})} + \sum_{n \geq 6} \frac{c_n}{T^{4-n}} O_n \right]. \tag{2.14}$$

In the above c_0 is a T-dependent "cosmological constant" of the 3d theory and corresponds to a shift in the free energy due to $\omega_n \neq 0$ loops [100]. It will be dropped in the following, because only free-energy differences matter for phase transitions. The sum over n contains higher-dimensional operators that appear naturally when integrating out heavy fields, but their couplings are suppressed by appropriate powers of πT. The overall factor of $1/T$ comes from a trivial τ-integral and could be absorbed in a redefinition of fields and couplings, $\phi \to \phi/\sqrt{T}, \bar{\lambda} \to T\bar{\lambda}$ and so on. Because the "natural", rescaled coupling has a positive mass dimension, the 3d theory is *super-renormalizable* if the higher-dimensional operators O_n are dropped by truncation.

In (2.14), the temperature appears merely as an overall scaling of the action and in the definitions of the renormalized parameters; for all practical purposes the EFT behaves like a zero-temperature field theory with Euclidean metric. Carrying out dimensional reduction corresponds to fixing the parameters $Z_\phi, \bar{m}^2, \bar{\lambda}, c_n$ so that the 3d EFT describes the same IR physics as the finite-T 4d theory. This can be done by requiring that off-shell Green's functions for the static modes match in both theories, for external momenta $p \ll \pi T$.[5] Integrating out the hard modes is equivalent to modifying counterterms of the zero modes, so we may solve the 3d parameters perturbatively by writing

$$Z_\phi = 1 + (\delta Z_\phi)_T, \qquad \bar{m}^2 = m^2 + (\delta m^2)_T, \qquad \bar{\lambda} = \lambda + (\delta\lambda)_T, \tag{2.15}$$

and treating the "thermal counterterms", denoted by a subscript T, as additional interactions in the matching calculation. "Normal" UV counterterms for canceling $1/\epsilon$ poles appear in $\mathcal{L}_{\rm ct}^{(3{\rm d})}$.

The matching of high-T correlators is not fundamentally different from standard EFT matching calculations at zero temperature, so we cut down on technical details here. Let us note that since the EFT approach makes sense only in the presence of a mass hierarchy $m \ll \pi T$, we may safely expand propagators with $\omega_n \neq 0$ in powers of m/T. This is the *high-T expansion* of sum-integrals. Matching the scalar theory at $O(\lambda)$ and at leading order in m/T gives

$$\bar{m}^2 = m^2 + \frac{\lambda T^2}{24} \tag{2.16}$$

$$\bar{\lambda} = \lambda \tag{2.17}$$

$$Z_\phi = 1, \tag{2.18}$$

[5] To reproduce the static S-matrix it suffices to match one-particle-irreducible (1PI) diagrams only, because it is not possible to construct reducible diagrams with $\omega_n = 0$ in the external legs and an $\omega_n \neq 0$ propagator in a reducible internal line.

and the higher-dimensional operators in (2.13) do not appear at this order. Eqs. (2.16) through (2.18) correspond to a 1-loop matching of the two-point function and a tree-level matching of the ϕ^4 interaction. At higher loop orders, one encounters diagrams with both $\omega_n = 0$ and hard modes in the loops, but these are absorbed on the EFT side by loop diagrams containing a "thermal counterterm" interaction. Detailed examples of matching in the high-T context can be found in *e.g.* [3, 93, 95, 99–102].

From (2.16) we see that the zero mode generates a T-dependent mass correction due to its interaction with the hard modes. $\bar{m}^2$ is called the *thermal mass* of ϕ and is renormalization group (RG) invariant at leading order in λ. This is because in 3d, there are no logarithmic divergences at one loop, and this statement carries over to more realistic theories like the SM. At order $O(\lambda^2)$ the thermal mass becomes scale dependent, and $\bar{\lambda}$ obtains a logarithmic dependence on T. For the scalar toy model, these corrections are given in [101].

2.3 On the accuracy of high-T dimensional reduction

The generation of a thermal mass has an important consequence for dimensional reduction itself. For exact dimensional reduction the higher-dimensional operators in (2.14) should vanish as $T \to \infty$.[6] But because the mass $\bar{m}^2$ appears in the relevant Green's functions, the couplings c_n are not independent of T, in fact they can grow without bounds as $T \to \infty$. Therefore there will always exist a mismatch of order $\bar{m}/T$ (raised to some power) between typical Green's functions in the full theory and the truncated EFT [103], except for in some special cases that are discussed in the reference. This is essentially a finite-T analogue of the hierarchy problem, but differs from the zero-temperature case in that it cannot be "cured" by fine-tuning the temperature-independent bare parameters, and in that the problem is not restricted to scalar fields (see section 3.2).

Fortunately, the aforementioned limitation does not render the 3d approach useless. This is because the T-dependent contribution in $\bar{m}^2$ is proportional to λ, meaning that the errors that do not vanish at infinite T are suppressed by powers of the coupling. Thus dimensional reduction can be accurate if the 4d theory is weakly coupled at the scale where the theories are matched [92], *i.e.* around $\bar{\mu} \sim \pi T$.[7] It is also easy to see that the operators of dimension six and higher appear first at $O(\lambda^3)$ and can thus be neglected at low orders of perturbation theory. This counting applies also to operators containing derivatives, if we assume $p \sim \lambda T$ for external momenta. Indeed, at $O(\lambda^2)$ only super-renormalizable operators are needed, and for weakly coupled theories the higher-order λ^3 corrections can be very small [93]. Concrete accuracy estimates are discussed in section 4.2.

2.4 Infrared sensitivity of finite-T perturbation theory

Dimensional reduction establishes that at high T, the IR behavior of a QFT is governed by super-renormalizable interactions. This has the pleasant consequence that the 3d EFT renormalizes

[6] Actually, some dimension-five and six operators (in 4d units) are renormalizable in 3d, and we should demand $T \to \infty$ decoupling of non-renormalizable operators only.

[7] The relevant matching scale in the SM is approximately $7T$, corresponding to the average momentum of integration over the hard modes [91].

nicely, and for instance the RG running can be solved exactly at the 2-loop level [91]. The downside of super-renormalizability is that perturbation theory is sensitive to IR physics, and will generally converge more slowly than at zero temperature. Because the effective coupling in 3d is $T\lambda$, to form a dimensionless expansion parameter we must combine this with a mass scale coming from 3d loop integrals. The only possible scale is $\bar{m}$, so perturbation theory for the Matsubara zero modes is an expansion in $T\lambda/\bar{m}$.

At extremely high temperatures the T^2 term in eq. (2.16) dominates, and the expansion parameter is

$$\frac{T\lambda}{\bar{m}} \sim \frac{T\lambda}{T\sqrt{\lambda}} \sim \sqrt{\lambda}. \tag{2.19}$$

Thus at high temperature, there is *less* suppression associated with a loop than in $T = 0$ perturbation theory. Physically, this means that the thermal bath boosts the interaction strengths of long-wavelength modes, and we can understand this phenomenon by considering particle occupation numbers (in a renormalized sense, so that virtual particles are not counted). At zero temperature, the number of particles is low, and the interactions occur between very few particles at a time. In contrast, at finite temperature the number of bosons participating in collisions follows the Bose-Einstein distribution

$$n_B(E) = \frac{1}{e^{E/T} - 1}, \tag{2.20}$$

so the effective coupling should be of order $\lambda n_B(E)$. Low-energy modes with $E \ll T$ feel enhanced interactions because then $n_B(E) \sim T/E \gg 1$. This discussion also demonstrates that perturbation theory for fermions, which get integrated out at high T, is insensitive to physics at distances $\ll T$, and that the bosonic IR sensitivity is not merely an artifact caused by the effective 3d description.

In scalar theories it may happen that the effective mass $\bar{m}$ vanishes, due to a cancellation between the vacuum m^2 and the thermal correction. This is precisely the situation in second-order phase transitions, where the system admits an infinite correlation length at the critical temperature. But at this temperature, $\bar{m} \to 0$ and $T\lambda/\bar{m} \to \infty$, and we cannot trust perturbation theory at all! More generally, there is no small expansion parameter if $m \leq \lambda T$, and the system needs to be studied non-perturbatively for reliable results. As discussed below, this may happen even in first-order transitions even though the correlation lengths remain finite.

The conclusion here is that a weakly-coupled theory at zero temperature may become non-perturbative once the temperature is turned on, but the coupling is strong only for specific long-wavelength modes that can be isolated in a simplified EFT setting.

Chapter 3

Aspects of gauge theories

Before discussing the full Standard Model at finite temperature, let us review some well-known properties of pure gauge theories with and without matter fields, and discuss in particular their high-T behavior. We also introduce the lattice formulation of gauge theories, which becomes relevant later on when we discuss the electroweak phase transition in a non-perturbative framework.

3.1 The Yang-Mills field

Both QCD and the electroweak theory are based on the notion of non-abelian gauge interaction, described by Yang-Mills theory. In Euclidean signature, the Yang-Mills Lagrangian reads

$$\mathcal{L}_{\mathrm{YM}} = \frac{1}{2}\,\mathrm{Tr}\,F_{\mu\nu}F_{\mu\nu}, \qquad \text{where} \qquad F_{\mu\nu} = \partial_\mu A_\nu - \partial_\nu A_\mu + ig[A_\mu, A_\nu]. \tag{3.1}$$

In this chapter we take the gauge group to be $G = \mathrm{SU}(N)$, so the gauge field A_μ is a vector in the associated Lie algebra $\mathfrak{su}(N)$. The gauge field can be written in different forms by specifying a basis of generators $T^a(R)$ in the Lie algebra, $A_\mu = A_\mu^a T^a(R)$, and we take the generators to be Hermitian by convention.

Gauge symmetry refers to invariance of the theory under the *local* transformations

$$A_\mu(x) \to \Omega(x)A_\mu(x)\Omega^{-1}(x) - \frac{i}{g}\Omega(x)\partial_\mu\Omega^{-1}(x), \tag{3.2}$$

where $\Omega(x) \in \mathrm{SU}(N)$. Gauge symmetry is to be understood as a redundancy in our description of the system rather than a true symmetry of the nature. This is evident already classically in the equations of motion, which specify the evolution of A_μ only up to gauge transformations. Describing the system in terms of redundant gauge degrees of freedom is nevertheless advantageous because it allows for a concise description of dynamics of (classically) massless spin-1 fields in terms of a local, Lorentz-invariant Lagrangian.

The presence of a gauge freedom means that only gauge-invariant quantities can be considered physical. In fact, there exists a theorem, due to Elitzur [104], stating that the expectation value of *any* gauge-dependent local quantity vanishes identically in a gauge-symmetric theory. Heuristically, this result arises because gauge transformations act on the fields locally and involve only very few degrees of freedom, preventing the formation of long-distance order that could be

interpreted as spontaneous breakdown of the local symmetry (there is not even short-range order!). Therefore $\langle O \rangle = 0$ always, if the operator O has non-trivial transformation properties under gauge transformations. However, it is well known that in order to define gauge theory in the perturbative context one needs to *explicitly* remove the gauge redundancy through gauge fixing; the gauge propagator $\langle A^a_\mu(x) A^b_\nu(y) \rangle$ is not well defined if the gauge symmetry is manifest. The gauge fixing need not preserve expectation values of generic, gauge-variant operators, as is evident in *e.g.* the popular Faddeev-Popov procedure. Thus in a gauge-fixed setting, one can have $\langle O \rangle \neq 0$ even if O is not a gauge-invariant operator, but such expectation values clearly cannot be regarded as physical observables.

The gauge field A_μ has a useful geometrical interpretation. Suppose we add a matter field, $\phi(x)$, transforming under some irreducible representation of the gauge group G. The allowed values of ϕ form a vector space at each spacetime point x, or a *fiber*. Gauge symmetry means that the basis vectors of the fiber can be chosen differently at different locations x and y, making a direct comparison of $\phi(x)$ and $\phi(y)$ meaningless. The role of the gauge field A_μ is to relate fibers on infinitesimally close spacetime points. In other words, A_μ is a connection that tells us how to parallel transport the field ϕ at point x to point $x + \delta x$. Infinitesimally, the parallel transport of field ϕ in representation R is

$$\phi(x) \to \left(1 - ig\delta x_\mu A^a_\mu(x) T^a(R)\right) \phi(x), \tag{3.3}$$

which produces a new vector with similar transformation properties as $\phi(x + \delta x)$. Parallel transports over longer distances can be constructed by repeated application of eq. (3.3), *e.g.* the transport from y to x along path C is carried out by the path-ordered exponential

$$U_C(x, y) = \mathcal{P} \exp[ig \int_C dx_\mu \, A^a_\mu T^a(R)]. \tag{3.4}$$

The object $U_C(x, y)$ is called a *Wilson line* along C. Wilson lines are the fundamental degrees of freedom in lattice gauge theory, as described below.

Quite remarkably, non-abelian gauge theories are strongly coupled in the IR and exhibit *confinement*: the physical spectrum consists of gapped (massive) composite objects. In contrast, at high energies the coupling is small, and perturbation theory can be reliable above the confinement scale. This is called *asymptotic freedom*. It is well known (and reviewed in [105]) that at finite temperature, the pure Yang-Mills theory undergoes a confinement-deconfinement phase transition that can be associated with spontaneous breakdown of the discrete center symmetry of the gauge group. However, this notion breaks down when matter fields in fundamental representation are present, because these explicitly break the center symmetry at the Lagrangian level. Indeed, in physical QCD the would-be deconfining transition is merely a smooth crossover [6], and the confining and deconfining "phases" are actually the same thermodynamical phase.

3.2 Yang-Mills theory at high temperature

In section 2.2 we argued that scalar field theories undergo effective dimensional reduction at high temperatures. The same is true for gauge fields, but the effective 3d theory admits a richer structure [90]. Gauge fields in 3d carry three spacetime components, while in 4d there is also the

(imaginary) time component A_0. Under static gauge transformations, its transformation law (3.2) reduces to

$$A_0 \to \Omega(x) A_0(x) \Omega^{-1}(x), \tag{3.5}$$

which is simply the gauge transformation of a scalar in the adjoint representation of SU(N). Thus we expect the high-T equilibrium description of 4d gauge fields to match that of a static theory with 3d gauge invariance and an adjoint scalar field. In the following we assume the theory to be sufficiently weakly coupled that perturbation theory makes sense, *i.e.* we probe energies above the confinement scale.

The dimensionally-reduced action corresponding to (3.1) reads (before gauge fixing)

$$S_E^{(3d)} = \int d^3x \Big\{ \frac{1}{2} \operatorname{Tr} F_{ij} F_{ij} + \operatorname{Tr} D_i A_0 D_i A_0 + m_D^2 \operatorname{Tr} A_0^2 + \lambda_A (\operatorname{Tr} A_0^2)^2 + \bar{\lambda}_A \operatorname{Tr} A_0^4 \Big\}, \tag{3.6}$$

where we moved directly to the natural 3d scaling of fields and parameters. The subscript in S_E refers to "electrostatic", and this terminology is explained below. In (3.6), F_{ij} is the 3d field strength and $D_i A_0 = \partial_i A_0 + ig[A_i, A_0]$ is a covariant derivative in the adjoint representation. The 3d gauge coupling is $\bar{g}$, and we denote the adjoint scalar by A_0 to emphasize its 4d origin. Some further comments regarding the form of (3.6) are now in order.

- We have dropped higher-dimensional operators from the EFT. By simple power counting, one can conclude that their leading contribution to the free energy is of order g^7.
- Since A_0 becomes a scalar field in the dimensionally-reduced EFT, we have written a mass term for it. But as A_0 is also the temporal gauge field in the finite-T theory, it may seem strange that such mass should emerge. This mass arises through thermal effects and is not prohibited by Slavnov-Taylor identities, because Lorentz symmetry is not manifest at finite T.
- In addition to the quartic interactions in eq. (3.6), one could write down a gauge-invariant cubic term $\operatorname{Tr} A_0^3$ (although it vanishes identically for SU(2)). However, this operator can only arise from dimensional reduction in association with non-zero chemical potentials [106–108].
- For SU(2) and SU(3), the two quartic interactions are not independent because $(\operatorname{Tr} A_0^2)^2 = 2 \operatorname{Tr} A_0^4$, and it suffices to include only one of them in the action.
- Since fermions get integrated out in dimensional reduction, any fermionic matter content present in the original 4d theory affects only the matching of parameters in (3.6), not the form of the EFT itself.

Matching of the high-T and effective theories proceeds analogously to the scalar field case. In pure SU(N) Yang-Mills, the results at $O(g^2)$ are [109]

$$m_D^2 = \frac{N}{3} g^2 T^2 \tag{3.7}$$

$$\bar{g}^2 = g^2 T \tag{3.8}$$

and there is also a correction to field renormalization, while λ_A and $\bar{\lambda}_A$ do not get matched at this order. We see that the temporal gauge-field component A_0 develops a mass of order gT. This phenomenon is actually familiar from classical plasma physics. In a thermal medium containing mobile charge carriers, the interaction potential between two charges, separated by distance r, is of the Yukawa form $V(r) \sim \exp[-r\mu_D]/r$, instead of the usual $1/r$ Coulomb behavior. This is known as *Debye screening*, and μ_D is called the Debye screening parameter. In analogy to electromagnetism, the field A_0 is frequently called the "color-electric" field, and we see that at finite T the associated interaction is precisely a Yukawa potential with screening parameter m_D.[8]

We may ask whether there is screening associated also with the "color-magnetic" fields A_i. At the *perturbative* level, the answer is no: such screening mass is prohibited by 3d gauge invariance. But in section 2.4 we saw that perturbation theory in 3d breaks down in the presence of light degrees of freedom. In gauge theory the high-T coupling is g^2T, so the expansion parameter associated with A_0 is $g^2T/m_D \sim g$. In contrast, the spatial gauge fields A_i are perturbatively massless and there is no small expansion parameter. We conclude that *the thermodynamics of Yang-Mills fields is non-perturbative at distances* $\gtrsim (g^2T)^{-1}$, and one expects to find confining behavior in the IR regime [44, 45]. This is known as the *Linde problem* of thermal field theory, and affects the free energy first at order g^6.

The scales gT and g^2T of electric and magnetic screening are known as the *soft* and *ultrasoft* scales, respectively. Because parametrically $g^2T \ll gT$ and because the soft scale is still perturbative, we may simplify the EFT (3.6) by integrating out the screened A_0 field. This leaves a 3d EFT of the pure Yang-Mills type that is valid at the ultrasoft scale,

$$S_M^{(3d)} = \int d^3x \, \frac{1}{2} \operatorname{Tr} F_{ij} F_{ij}, \tag{3.9}$$

where the squared gauge coupling differs from g^2T by corrections of order g^3. In this way, the non-perturbative physics associated with the ultrasoft scale can be studied in a simplified setting. For SU(3), the EFTs (3.6) and (3.9) are called electrostatic and magnetostatic QCD, respectively. Their relevance for modern applications in thermal QCD is reviewed in [112].

3.3 Gauge theory on a Euclidean lattice

Because of the IR sensitivity of finite-T field theory, light bosons at finite temperature require non-perturbative treatment. The appropriate framework for non-perturbative investigations is that of lattice QFT, which we review here. We will ultimately apply the formalism to dimensionally-reduced EFTs, which are bosonic by construction, so for the most part our discussion of lattice fields will be restricted to bosons. We assume a hypercubic Euclidean lattice with homogeneous spacing a in all directions.[9]

Putting a QFT on a discrete lattice regulates functional integrals of the type (2.7) at the non-perturbative level, turning them into ordinary Riemann integrals and giving a precise mathematical meaning to the path integral measure. We denote the measure by $[d\phi] \equiv \prod_x d\phi(x)$ when

[8] At higher orders in g the definition of the physical Debye screening parameter is no longer unique, see [110, 111].

[9] Non-zero temperature can be introduced by making one direction periodic, and often the lattice spacing is chosen differently in this direction. This will not be relevant for our purposes, because the temperature dependence is accounted for in dimensional reduction.

referring to a lattice theory, and $\mathcal{D}\phi$ in the continuum context. The lattice spacing also introduces a natural momentum cut-off, as the discretized theory is unable to probe distance scales shorter than a. Thus the theory is insensitive to fluctuations at energy scales $\gtrsim 1/a$ and there are no explicit UV divergences. If we further introduce an IR cutoff, *i.e.* study the theory in a finite volume, it becomes possible to evaluate Euclidean correlation functions

$$\langle O \rangle = \frac{\int [d\phi]\; O e^{-S(\phi)}}{\int [d\phi]\; e^{-S(\phi)}} \tag{3.10}$$

numerically on a computer, at least in principle, without relying on perturbative expansions. Thus non-perturbative phenomena can be approached from first principles in a numerical manner via lattice simulations.

For scalar fields, writing down a lattice analogue of a given continuum QFT is straightforward. We let the field $\phi(x)$ take values on the lattice sites x, substitute derivatives with finite differences between nearest points and replace $\int d^d x \to a^d \sum_x$. Putting gauge fields on the lattice, on the other hand, is less trivial because a naive replacement of covariant derivatives with differences turns out to break gauge invariance. A better way is to implement the gauge field not as a connection A_μ, but directly as a parallel transporter $U_\mu(x)$ from site $x+\mu$ to x [113]. We adapt a standard notation where $x+\mu$ refers to the next lattice site from x in direction μ. In terms of a (fundamental) Wilson line (3.4),

$$U_\mu(x) = U(x, x+\mu) = e^{iagA_\mu(x)}. \tag{3.11}$$

The SU(N) valued object $U_\mu(x)$ is called a *gauge link*. It transforms under gauge transformations as

$$U_\mu(x) \to \Omega(x) U_\mu(x) \Omega^{-1}(x+\mu). \tag{3.12}$$

The gauge links can be combined with matter fields to form gauge-invariant objects. For instance, if ϕ is a scalar in the fundamental representation of SU(N), the parallel-transported difference

$$\hat{D}_\mu \phi(x) \equiv \frac{1}{a}\Big(U_\mu(x)\phi(x+\mu) - \phi(x)\Big) \tag{3.13}$$

transforms covariantly under gauge transformations, and for small a we have

$$a^d \sum_{x,\mu} \Big(\hat{D}_\mu \phi(x)\Big)^\dagger \Big(\hat{D}_\mu \phi(x)\Big) = \int d^d x\; (D_\mu \phi)^\dagger (D_\mu \phi) + O(a^2). \tag{3.14}$$

So we recover the continuum covariant kinetic term in the limit $a \to 0$.

To account for dynamics of the gauge links we must write down a gauge-invariant operator that agrees with $\operatorname{Tr} F_{\mu\nu} F_{\mu\nu}$ in the continuum limit. The simplest choice is to consider a closed Wilson loop over an elementary square on the lattice. This is known as the *Wilson plaquette*:

$$P_{\mu\nu}(x) = U_\mu(x) U_\nu(x+\mu) U_\mu^\dagger(x+\nu) U_\nu^\dagger(x), \tag{3.15}$$

which for small a behaves as $P_{\mu\nu} \sim \exp[iga^2 F_{\mu\nu}]$. The Euclidean SU($N$) Wilson gauge action reads, in d dimensions,

$$S_W = \frac{2N}{g^2 a^{4-d}} \sum_{x, i<j} \left[1 - \frac{1}{N} \operatorname{Re} \operatorname{Tr} P_{\mu\nu}(x)\right] = \int d^d x\; \frac{1}{2} \operatorname{Tr} F_{\mu\nu} F_{\mu\nu} + O(a^2 g^2). \tag{3.16}$$

The trace is taken to form a gauge-invariant object. The action (3.16) is the one used in this thesis and in associated publications. Both the gauge action and the bosonic kinetic term (3.14) have discretization errors of order a^2. It is possible to construct more complicated actions with smaller cut-off dependence using Symanzik improvement [114], but for bosonic theories in the dimensionally-reduced context this improvement would typically be overshadowed by $O(a)$ errors in lattice continuum relations. Further discussion appears in section 7.1.

In lattice regularization, the fundamental gauge degrees of freedom are the parallel transporters $U_\mu(x)$, (elements of SU(N)), instead of the Lie-algebra valued "gauge fields" A_μ. For meaningful functional integration we must specify what is meant by integration over the $U_\mu(x)$. A natural definition of the integration measure is given by the gauge-invariant Haar measure on the group manifold (see *e.g.* [115]). This has an important consequence, as because the functional integration is now performed over the compact SU(N) group, it is finite and well defined without the need to single out representatives of the gauge orbit. In other words, *there is no need for gauge fixing in the lattice theory*. Therefore the lattice framework provides a formulation of gauge theory that is unaffected by gauge-fixing difficulties at the non-perturbative level (the Gribov-Singer ambiguity [116, 117]), unless one is specifically interested in unphysical gauge-dependent quantities.

Let us mention briefly the role of fermions in lattice gauge theory. Discretization is notoriously complicated when fermions are present. In fact, there is no generally accepted lattice formulation of fermions that couple *chirally* to non-abelian gauge fields in four dimensions [118, 119], although proposed frameworks exist [120]. This means that no unambiguous lattice formulation exists for the SM, because the associated SU(2) interaction affects only left-handed fermions. This shortcoming makes direct lattice simulations of the full EW theory unpractical, but is avoided in the dimensionally-reduced approach where fermions get integrated out at the perturbative level.

Chapter 4

The Standard Model at finite temperature

Mathematically, the Standard Model is a non-abelian chiral gauge theory with gauge group SU(3)× $\mathrm{SU}(2)_L \times \mathrm{U}(1)_Y$, where the subscript L means that only left-handed fermions transform non-trivially under the $\mathrm{SU}(2)_L$ group, and the subscript Y refers to hypercharge. SU(3) corresponds to the strong QCD interaction while fields charged under $\mathrm{SU}(2)_L \times \mathrm{U}(1)_Y$ form the electroweak (EW) sector. A crucial ingredient is the Higgs field ϕ, which enters in the fundamental representation of $\mathrm{SU}(2)_L$ and carries hypercharge $\frac{1}{2}$.

At zero temperature, the $\mathrm{SU}(2)_L$ gauge bosons and fermions (apart from neutrinos) obtain tree-level masses due to the Higgs mechanism. There are three generations of fermions, but for the discussion of EWPT we may treat all but the heaviest top quark as being massless. This is because the masses are proportional to Yukawa couplings, and the top Yukawa $y_t \sim 1$ is orders of magnitude larger than that of other fermions and gives by far the dominant loop corrections to the Higgs potential. The SU(3) sector couples to the Higgs first through two-loop diagrams and does not play a major role in the following discussion.

The EW Lagrangian is, in Euclidean signature,

$$\begin{aligned} \mathcal{L}_{\mathrm{EW}} &= \frac{1}{2}\operatorname{Tr} F_{\mu\nu}F_{\mu\nu} + \frac{1}{4}B_{\mu\nu}B_{\mu\nu} + |D_\mu\phi|^2 + V(\phi) \ \ + (\text{fermions and Yukawas}), \\ V(\phi) &= m_\phi^2\phi^\dagger\phi + \lambda(\phi^\dagger\phi)^2, \end{aligned} \tag{4.1}$$

where $D_\mu\phi = (\partial_\mu + igA_\mu + \frac{1}{2}ig'B_\mu)\phi$, and the field strengths are

$$F_{\mu\nu} = \partial_\mu A_\nu - \partial_\nu A_\mu + ig[A_\mu, A_\nu] \quad (\text{for } \mathrm{SU}(2)_L) \tag{4.2}$$

$$B_{\mu\nu} = \partial_\mu B_\nu - \partial_\nu B_\mu \qquad\qquad (\text{for } \mathrm{U}(1)_Y). \tag{4.3}$$

To define the quantum theory in a perturbative setting, we must introduce a gauge-fixing condition. This can be *e.g.* a renormalizable R_ξ gauge implemented according to the Faddeev-Popov procedure, but we will not go into details as the methods are standard. What matters for the following is that the gauge is now fixed, meaning that gauge-dependent quantities may develop non-vanishing expectation values without contradicting Elitzur's theorem.

A further assumption in the SM is that $m_\phi^2 < 0$, so that a Higgs mechanism can take place. At tree level, the ground state of the Higgs potential lies at

$$\phi^\dagger \phi = -\frac{m_\phi^2}{2\lambda}. \tag{4.4}$$

The doublet ϕ may be parametrized as

$$\phi = \frac{1}{\sqrt{2}} \begin{pmatrix} G_2 + iG_1 \\ h - iG_3 \end{pmatrix} \tag{4.5}$$

and in suitable gauges (such as the R_ξ gauge) it is possible to introduce a background field v through $h \to h + v$, so that

$$\langle \phi \rangle = \frac{1}{\sqrt{2}} \begin{pmatrix} 0 \\ v \end{pmatrix}. \tag{4.6}$$

The gauge bosons and fermions then obtain masses proportional to v, and we say the gauge symmetry is "spontaneously broken" (in reality the gauge freedom was removed already in gauge fixing). The fields G_i then resemble Goldstone modes of a broken global symmetry, but we emphasize again that this picture is gauge dependent.[10] Without gauge fixing, and for instance in the temporal gauge [122], the Higgs VEV vanishes identically and a different description of the Higgs mechanism is required.

4.1 Phase structure of the electroweak theory

Consider now the SM at finite temperature. We are interested in what happens in the Higgs sector once the temperature reaches the GeV range, and this investigation is motivated by the following observation. Once the temperature is turned on, the Higgs mass parameter m_ϕ^2 obtains a quadratic T-dependent correction (similarly to eq. (2.16)) and remarkably, the correction turns out to be positive. This means that the thermally-corrected parameter $m_\phi^2(T)$ changes sign at some temperature $T_{\rm EW}$, and we expect the minimum of $V(\phi)$ to shift to the origin. In other words, at temperatures $T > T_{\rm EW}$ the Higgs mechanism should be inactive and the $\mathrm{SU}(2)_L$ gauge bosons perturbatively massless. The physical Higgs excitation has mass $M_h \approx 125$ GeV, fixing the zero-temperature parameter to be $m_\phi^2 \sim (100\ \mathrm{GeV})^2$. Thus the Higgs mechanism should be triggered at $T_{\rm EW} \sim 100$ GeV, and the question is, is there a phase transition at $T_{\rm EW}$?

Let us simplify the discussion by dropping fermions from the theory and focus only on the bosonic sector. At finite temperature this simplification is actually justified, because at high-T the IR physics is governed by a dimensionally-reduced bosonic theory. Fermionic corrections modify the long-distance coefficients of this effective theory, but we do not expect the phase diagram to be qualitatively affected. The technical reason for neglecting fermions is that there is then no ambiguity in formulating the theory non-perturbatively on the lattice, and we can make very

[10] Depending on the gauge choice, there may remain global "remnant" symmetries that can be broken spontaneously. However, neither the remnant symmetry group nor the resulting "phase diagram" are unique, *i.e.* they are gauge dependent [121].

general, albeit qualitative statements about the high-T behavior of this idealized $\mathrm{SU}(2) \times U(1)_Y$ + Higgs system.

We expect the high-T phase of the theory to resemble that of an asymptotically-free Yang-Mills theory with matter in fundamental representation. In particular, and as mentioned in section 3.1, there exists no symmetry that could distinguish between the confining and deconfining "phases". Thus we simply say that $T > T_{\mathrm{EW}}$ is the confining phase, and the spectrum is created by composite operators.[11] In fact, a theorem due to Osterwalder and Seiler [123] (also by Fradkin and Shenker [124]) states that if the Higgs field is in the fundamental representation, then *there is no clear distinction between the confining and Higgs phases* either; they are the same thermodynamical phase. The proof is based on lattice gauge theory and demonstrates that the confining and Higgs regimes can be analytically connected, and that no gauge-invariant, local order parameter exists that could distinguish between confinement and the Higgs mechanism.[12] There can, of course, be *quantitative* differences between the Higgs and confinement regimes, just like liquid water is quantitatively different from vapor even though the phases are analytically connected.

This discussion leads to a somewhat unconventional picture of the EW interaction. Because the confining and Higgs regimes are actually the same phase, the SU(2) sector must, in some sense, be confined at low temperatures as well, while at the same time the long-distance dynamics is made perturbative by the Higgs mechanism. This is sometimes called *Higgs-confinement complementarity*. In particular the spectrum should consist of gapless, SU(2) singlet composite operators instead of *e.g.* asymptotic Higgs particles and W, Z bosons.[13] Local operators describing these bound states have been written down in [127–130]. In [129, 130], perturbation theory based on these gauge-invariant operators was developed, showing for instance that the gauge-invariant pole masses are in one-to-one correspondence with those predicted by the "standard" approach obtained by perturbing the Higgs field around a gauge-fixed background. Thus there is no discrepancy with the standard approach, although the terminology is very different. A review of these concepts appears in [131].

The main message of this discussion is that the EW theory can be understood as a confining theory, akin to QCD, where the physical excitations are gauge-invariant composite objects constructed from the elementary fields $(A_\mu, B_\mu, \phi, \dots)$. The main difference to QCD is that because of Higgs mechanism, the EW theory admits a reliable perturbative expansion at zero temperature [129, 130]. These realizations are crucial for understanding the theory at the non-perturbative level and without referring to gauge-dependent concepts like the Higgs VEV, which carry no meaning in the manifestly gauge-invariant lattice formulation. Non-perturbative methods, in turn, are needed at finite temperature due to the Linde problem and the overall IR sensitivity of finite-T perturbation theory.

[11] There remains a massless photon from the hypercharge U(1) interaction, which does not confine.

[12] It has recently been demonstrated that a clear phase boundary can exist if the theory admits an additional global symmetry that is spontaneously broken in *both* the confining and Higgs regimes [125]. This mechanism may have far-reaching consequences also for the EW phase structure in certain BSM extensions.

[13] One may wonder if the entire spectrum of the SM could be described through genuine strong-coupling effects in the SU(2) sector, so that the perturbative Higgs mechanism would not be needed. Historically, this was attempted by the Abbott-Farhi model [126] and leads to vastly different phenomenology from the SM case at energies $\gtrsim$ 100 GeV. Thus the correct description of EW interactions seems to require the Higgs mechanism.

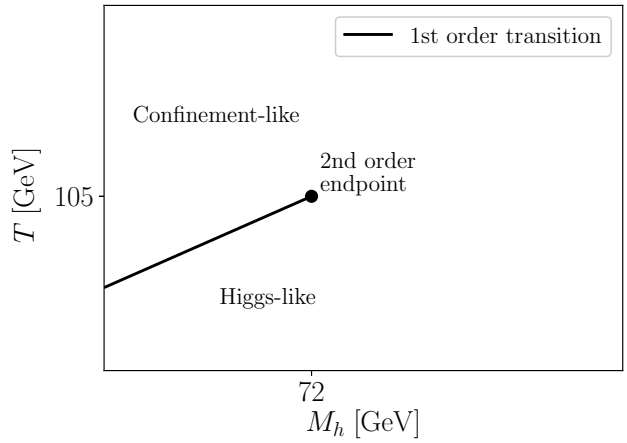

Figure 4.1: Schematic phase diagram for the electroweak theory. If the Higgs excitation was lighter than around 72 GeV, there would be a first-order phase transition at $T \approx 100$ GeV. The line of first-order transitions ends at a critical point, after which there is only a smooth crossover from the confinement-like regime to the low-T Higgs regime. There is no qualitative change in the theory across the crossover, and the spectrum in both regimes is described by gauge-invariant composite operators.

After this lengthy preamble, let us qualitatively discuss the phase diagram of the standard EW theory (at vanishing chemical potentials), illustrated in fig. 4.1. For historical and phenomenological convenience we express it in a (M_h, T)-plane, with M_h denoting the mass of the physical Higgs excitation. At small Higgs masses, there exists a first-order transition between the confining and Higgs regimes, and across this transition the screening masses and various correlation lengths change discontinuously. This is known from non-perturbative lattice simulations [85, 86, 132], and in this part of the diagram, finite-T perturbation theory is considered at least qualitatively reliable [133–135]. Because the "phases" are analytically connected, the line of first-order transitions must end at a critical endpoint, at which the transition is of second order and the Higgs field develops an infinite correlation length. Thus a precise determination of this endpoint is an inherently non-perturbative problem.

According to numerical simulations both in the dimensionally-reduced EFT [7, 87, 136] and in the 4d SU(2) + Higgs theory [8, 132], the endpoint lies approximately at $M_h^{(\mathrm{crit})} \approx 72$ GeV. Critical behavior at the endpoint belongs to the Ising universality class [137]. For $M_h > M_h^{(\mathrm{crit})}$ and in particular for the experimentally-confirmed value $M_h = 125$ GeV, there is no transition whatsoever, and the finite-T theory resembles a supercritical fluid. Around $T \sim 100$ GeV the theory undergoes rapid but smooth changes in its correlation functions. This behavior is called the EW crossover, and the associated temperature is typically defined as the point where the susceptibility of $\langle \phi^\dagger \phi \rangle$ is at maximum. For the physical Higgs mass, the crossover happens at

$T_{\rm EW} \approx 160$ GeV [88].

Very frequently, the high-T confinement-like regime is called the "symmetric phase" and the low-T Higgs-like regime the "broken phase". This terminology is notoriously misleading, as (i) there is only one phase, and (ii) there is no symmetry breaking or restoration. But because this abuse of language is convenient and common in the literature, we also adapt these labels in the following discussion. We will also refer to the transition from confinement-like behavior to the Higgs regime as the electroweak phase transition (EWPT), even if there is actually a smooth crossover.

4.2 Dimensionally-reduced theory for the hot Standard Model

Let us return to the perturbative setting, so that the gauge-fixed Higgs VEV v is as in (4.6) at low temperatures and vanishes for $T > T_{\rm EW} \sim 100$ GeV. For concreteness, focus now on the symmetric high-T regime. Calculating the finite-T self-energy correction for the Higgs doublet, we find that the loop-corrected mass parameter behaves parametrically as $m^2(T) \sim m_\phi^2 + g^2T^2$, where g^2 denotes a generic quartic coupling. The perturbative Higgs mechanism is triggered when $m^2(T) \sim 0$, or $m_\phi^2 \sim -g^2T^2$. In other words the scalar excitations are parametrically light near $T_{\rm EW}$, while the gauge bosons are perturbatively massless in the symmetric regime. Thus the theory can be dimensionally-reduced in the IR, at distances $\gg 1/T$.

The appropriate 3d EFT is a straightforward generalization of those described in sections 2.2 and 3.2. The time components of gauge fields experience Debye screening, so we include an SU(2) adjoint scalar $A_0 = \frac{1}{2}\sigma^a A_0^a$ and a $\mathrm{U}(1)_Y$ singlet B_0. The 3d action is

$$\begin{aligned} S^{(3d)} = \int d^3x \Big\{ & \frac{1}{2}\,\mathrm{Tr}\, F_{ij}F_{ij} + \frac{1}{4}B_{ij}B_{ij} + (D_i\phi)^\dagger(D_i\phi) + \frac{1}{2}(D_iA_0^a)^2 + \frac{1}{2}(\partial_i B_0)^2 \\ & + m_{\phi,3}^2\phi^\dagger\phi + \lambda_3(\phi^\dagger\phi)^2 + \frac{1}{2}m_D^2 A_0^a A_0^a + \frac{1}{2}(m_D')^2 B_0^2 \\ & + h_1\phi^\dagger\phi A_0^a A_0^a + h_2\phi^\dagger\phi B_0^2 + h_3\phi^\dagger A_0^a\sigma^a\phi B_0 + (\text{interactions among } A_0, B_0)\Big\}. \end{aligned} \tag{4.7}$$

There are no fermions, because they get integrated out in dimensional reduction.

At this stage it is convenient to introduce a schematic power counting for the numerous coupling constants in the EW theory. These are the gauge couplings g, g', the Higgs quartic coupling λ and the top Yukawa y_t. Renormalization structure suggests the counting $\lambda \sim y_t^2 \sim g'^2 \sim g^2$, which is not terribly accurate numerically as, for instance, $y_t^2 \sim 1 \gg 0.4 \sim g^2$, but is useful when discussing parametric corrections from loops. 1-loop dimensional reduction renormalizes mass parameters at $O(g^2)$ and quartic couplings at $O(g^4)$, at 2-loop order the mass corrections are $O(g^4)$, and so on. The EFT (4.7) is suitable for describing EW thermodynamics at the soft scale gT.

The next task it to match the parameters in (4.7) to those in the full 4d theory. At leading g^2

order, the results are [93, 95]:

$$m_{\phi,3}^2 = m_\phi^2 + \frac{T^2}{16}\left(3g^2 + g'^2 + 4y_t^2 + 8\lambda\right) \tag{4.8}$$

$$m_D^2 = g^2T^2\left(\frac{5}{6} + \frac{N_f}{3}\right) \tag{4.9}$$

$$(m_D')^2 = g'^2T^2\left(\frac{1}{6} + \frac{5N_f}{9}\right) \tag{4.10}$$

$$h_1 = \frac{1}{4}g^2T \tag{4.11}$$

$$h_2 = \frac{1}{4}g'^2T \tag{4.12}$$

$$h_3 = \frac{1}{2}gg'T, \tag{4.13}$$

and trivially $\lambda_3 = \lambda T$, $g_3^2 = g^2T$, $(g_3')^2 = g'^2T$. In the above, $N_f = 3$ is the number of fermion generations. For brevity, we do not write down the $O(g^4)$ corrections. These are given in [93] apart from terms of order $g^2g'^2$ and g'^4, and to full $O(g^4)$ accuracy in [95]. Two-loop corrections to the Debye masses can be read from [138].

Near $T \approx T_{\rm EW}$, the thermal Higgs mass $m_{\phi,3}^2$ is small because the vacuum contribution m_ϕ^2 gets partially canceled by the thermal correction. We express this parametrically as $m_{\phi,3} \lesssim g^2T$. In the temperature range where this hierarchy holds, the Higgs field is strongly coupled: no small expansion parameter exists because ratios of the form $g^2T/m_{\phi,3}$ are unsuppressed. Thus we expect perturbation theory to break down precisely at the most interesting temperatures! On the other hand we have the hierarchy $m_{\phi,3} \lesssim m_D, m_D'$, so the scalars A_0 and B_0 may be integrated out as in section 3.2 (this is why we did not bother writing down their interactions in (4.7)). This procedure corrects the remaining parameters at $O(g^3)$ and considerably simplifies the EFT:

$$\bar{S}^{(3\mathrm{d})} = \int d^3x \left\{\frac{1}{2}\,\mathrm{Tr}\,F_{ij}F_{ij} + \frac{1}{4}B_{ij}B_{ij} + (D_i\phi)^\dagger(D_i\phi) + \bar{m}_{\phi,3}^2\phi^\dagger\phi + \bar{\lambda}_3(\phi^\dagger\phi)^2\right\}. \tag{4.14}$$

The matching relations for this EFT can be found in [93, 95]. The theory is formally valid at the ultrasoft scale g^2T, and we denote its parameters by an additional overline ($\bar{g}_3$ *etc*). To summarize, around $T \sim 100$ GeV the equilibrium behavior of the EW theory is that of a 3d $\mathrm{SU}(2) \times \mathrm{U}(1)_Y$ + Higgs system.

The theory (4.14) has been studied non-perturbatively in [85, 86] using lattice simulations. Its phase structure depends on three dimensionless ratios

$$x \equiv \frac{\bar{\lambda}_3}{\bar{g}_3^2}, \qquad y \equiv \frac{\bar{m}_{\phi,3}^2}{\bar{g}_3^4}, \qquad z \equiv \frac{(\bar{g}_3')^2}{\bar{g}_3^2}. \tag{4.15}$$

Temperature dependence of x and z is only logarithmic and can be neglected to reasonable accuracy. x depends on M_h according to the relations in [85], and we fix z to its physical value of roughly $z = 0.3$. If $0 < x \lesssim 0.11$, the simulations reveal a first-order EWPT occurring near $y \approx 0$. It is strong for small $x \lesssim 0.036$, and by "strong" we mean the baryogenesis criterion that the

gauge-fixed VEV has discontinuity $\Delta v/T \gtrsim 1$.[14] The transition ends at a critical value $x_c \approx 0.11$, and at larger values there is just a smooth crossover. For the physical Higgs mass we find $x \approx 0.3$, and the theory lies deep in the crossover region.

How accurately can we trust the EFT (4.14)? In the perturbative matching calculation it was implicitly assumed that we can expand around $\phi = 0$, *i.e.* treat gauge fields and fermions as being massless. In the "symmetric phase" this is a good approximation because the SU(2) sector is asymptotically free, but for studying transitions between "symmetric" and "broken" regimes it is crucial that we can trust the 3d description also when the VEV is non-vanishing. But because the two regimes are analytically connected, there is no fundamental issue in expanding around $\phi = 0$; we only need to make sure that the neglected background-dependent corrections remain small. These arise from higher-dimensional operators that were dropped in the reduction process.

To be more specific, the true effective theory produced by dimensional reduction is one that contains all possible operators, including higher-dimensional ones like $c_6(\phi^\dagger\phi)^3$. Shifting $\phi^\dagger\phi \to \phi^\dagger\phi + v^2$, this operator modifies the coefficients of lower-order operators $\phi^\dagger\phi$ and $(\phi^\dagger\phi)^2$ by terms proportional to $c_6 v^4$, $c_6 v^2$, but the form of the theory is unchanged. We may perform the same shift in the truncated theory (4.7) (or (4.14)), but modifications from the higher-dimensional operators will be missing because they were dropped in the reduction process. Thus expanding around $\phi = 0$ is equivalent to assuming that the higher-dimensional operators are small enough to be neglected also after introducing a non-zero background field. In other words, the background-dependent masses $m(v)$ should respect the hierarchy $m(v) \ll \pi T$.

Because masses in the broken phase are parametrically $m(v) \sim gv$, we clearly cannot expect the EFT to work deep in the Higgs regime where $v \gg \pi T$. However, at smaller field values the 3d approach turns out to work very well. This was estimated perturbatively in [93] by considering the dominant[15] higher-dimensional operator $(\phi^\dagger\phi)^3$, which appears in the EFT at order g^6. For $v \sim T$, this operator causes a relative shift of less than 1% in the Higgs VEV, suggesting that the truncated theory (4.14) is accurate within one percent for typical quantities in the Higgs regime near $T_{\rm EW}$. The error is dominated by the top quark, whose mass is numerically close to T after the Higgs mechanism. In particular, the neglected higher-order corrections from integrating out A_0 and B_0 are completely overshadowed by the $O(1\%)$ errors associated with the top Yukawa coupling.

4.3 First-order electroweak phase transition from parametrically heavy fields?

A convenient property of effective theories is that they admit a degree of universality: different theories may look qualitatively the same at long distances once heavy excitations are integrated out. With this realization, we may utilize the EFT (4.14) to make model-independent statements

[14] This condition is sloppy, and meaningful only at the (semi-)classical level. For a more physical measure of transition strength that is relevant for baryogenesis, one has to study discontinuities in gauge-invariant expectation values and their relation to the suppression of electroweak sphalerons [139].

[15] There are gauge-invariant operators at dimension five, but these do not arise in dimensional reduction of the SM [108].

about the EWPT in theories where the new degrees of freedom are considerably heavier than the SM Higgs.

Near temperatures $T_{\rm EW} \sim 100$ GeV where the phase transition would occur, the theory develops a natural scale hierarchy, $g^2 T \ll gT \ll \pi T$. Here we assume that as the EWPT takes place, the new field are sufficiently heavy and cannot participate in the long-distance dynamics of the transition. We may then proceed with the 3d approach, integrating out the hard Matsubara modes but also the heavy BSM excitations. Specifically, we assume that the new fields have mass $\gtrsim gT$ at the phase-transition point. Then the resulting EFT is of the familiar form (4.14), but the parameters x, y, z in (4.15) differ from their SM values because of corrections from the BSM fields. Indeed, the phase transition still happens at $y \approx 0$, but at the same time x can be small, and a first-order EWPT becomes an option.

In this way, near the critical temperature we can reduce any (perturbative) extension of the SM with parametrically heavy BSM fields to a simple 3d theory of the form (4.14), and recycle the non-perturbative results of [85, 86] to deduce the order of the phase transition. Technically, this amounts to assuming the new fields to be heavy enough that the neglected higher-dimensional operators are small and negligible. The meaning of "heavy" here is dependent on the context. Suppose we have a new scalar Φ, coupled to the Higgs through a quartic interaction of the form $\lambda_{\rm BSM}\phi^\dagger\phi\Phi^2$. Integrating Φ out at the soft scale, it contributes to the dominant dimension-six operator $c_6(\phi^\dagger\phi)^3/T^2$ parametrically as $c_6 \sim (T\lambda_{\rm BSM}/m_{\rm BSM})^3$, which is small if we require $m_{\rm BSM} \gg \lambda_{\rm BSM} T$. If the coupling $\lambda_{\rm BSM}$ is large, the new scalar may need to be quite heavy for the method to be reliable.

We applied this approach to various BSM theories in [94–97]. A common finding was that the EWPT remains a crossover when the BSM couplings to the Higgs are small, but can become a first-order transition at larger couplings $\lambda_{\rm BSM} \sim O(1)$. This is illustrated in fig. 4.2 for a SU(2)-triplet extended model [96] (the Lagrangian is given in eq. (7.4) below). In the figure, M_Σ refers to the vacuum mass of the neutral BSM excitation and a_2 is a quartic coupling with the Higgs. The method is not very accurate deep in the first-order region, because the higher-dimensional operators are not negligible anymore when x is small, and the approach breaks down altogether when $x < 0$, as the EFT becomes unstable at tree level.[16] The boundary between crossover and first-order transitions can be found with $10\% - 30\%$ accuracy.

The paper [97] discusses gravitational-wave production, assuming a strong transition (small x) within the IR effective theory (4.14). This analysis utilizes non-perturbative results of [140], where the real-time rate of bubble nucleation was computed in this EFT, and the fluid simulations of [30]. Knowing the nucleation rate allows one to determine the duration of the EWPT, or the temperature range during which bubbles collide and produce gravitational waves. The conclusion in [97] is that any first-order phase transition described by the super-renormalizable EFT (4.14) is necessarily too weak and ends too quickly for the resulting gravitational-wave signal to be observable in LISA, or in other planned detectors.

While these results seem discouraging, they rely on the assumption that BSM effects decouple, to good approximation, from the long-distance physics of the EWPT. At the same time, this

[16] In the figure, "DR" refers to dimensional reduction, while strictly speaking it is the assumption of a non-dynamical triplet field that breaks down in the $x < 0$ region.

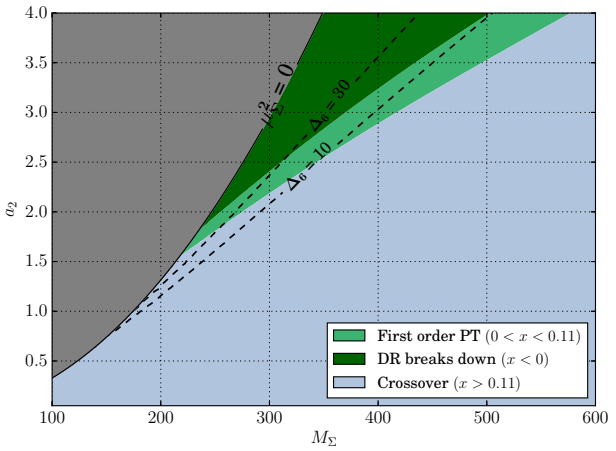

Figure 4.2: Qualitative phase diagram for a real-triplet scalar extension of the SM, obtained by integrating out the triplet excitations near T_c and applying the non-perturbative results of [85, 86]. First-order EWPT (light green region) is found to occur at relative large values of the Higgs-to-triplet quartic coupling a_2. Dark green region is where the EFT (4.14) is unstable, and integrating out the triplet is no longer justified. This is reflected by the dashed lines, which measure the relative importance of neglected higher-dimensional operators, *e.g.* $\Delta_6 = 10$ means that the error is roughly 10%. The gray region is where the triplet can exhibit a Higgs mechanism of its own, and was not explored. Figure is from ref. [96], where further details can be found.

model-independent investigation shows that the decoupling is only marginal if the transition is of first order, because the higher-dimensional operators cannot be neglected in this case. The results of [97] can be taken as a concrete indicator that a strong first-order EWPT is possible only if the new fields actively participate in the thermodynamics. Thus there is need to keep the new fields explicitly present in the 3d EFTs and eventually include them in new non-perturbative lattice simulations.

Chapter 5

Perturbative analysis in a real-singlet extended model

Before attempting fresh non-perturbative investigations in concrete BSM models, it is worthwhile to explore analytical methods for describing the EWPT. Although the transition necessarily involves non-perturbative physics at least in the symmetric phase, we may apply perturbation theory as a first approximation. The motivation here is pragmatic: comprehensive non-perturbative simulations require immense numerical effort and are not suited for large-scale parameter-space scans in BSM settings, which often involve more than one free parameter. Here we describe the conventional perturbative approach to the EWPT using the *effective potential* and demonstrate the importance of corrections beyond the 1-loop level. This chapter is based on [3], where we studied the effective potential at 2-loop order in a model involving a new gauge singlet.

5.1 The singlet model

Perhaps the simplest possible extension of the SM is obtained by adding a real singlet scalar S. We refer to this model as xSM. The Lagrangian reads

$$\mathcal{L} = \mathcal{L}_{\text{SM}} + \frac{1}{2}(\partial_\mu S)^2 + b_1 S + \frac{1}{2}m_S^2 S^2 + \frac{1}{3}b_3 S^3 + \frac{1}{4}b_4 S^4 + \frac{1}{2}a_1 S\phi^\dagger\phi + \frac{1}{2}a_2 S^2\phi^\dagger\phi. \tag{5.1}$$

The most general scalar potential contains a linear "tadpole" term b_1 and cubic interactions a_1, b_3, but one of these can be removed by performing a constant shift in the singlet field. We may, for instance, demand $\langle S\rangle = 0$ at tree level. Thus the theory contains five free parameters beyond those that can be fixed by SM measurements.

If we write the Higgs doublet as

$$\phi = \frac{1}{\sqrt{2}}\begin{pmatrix} G_2 + iG_1 \\ v + h - iG_3 \end{pmatrix}, \tag{5.2}$$

where v is the gauge-fixed VEV, the mass eigenstates h_1, h_2 will in general be mixtures of h and S. We write these as

$$\begin{pmatrix} h_1 \\ h_2 \end{pmatrix} = \begin{pmatrix} \cos\theta & -\sin\theta \\ \sin\theta & \cos\theta \end{pmatrix}\begin{pmatrix} h \\ S \end{pmatrix}, \tag{5.3}$$

where the mixing angle θ is chosen to diagonalize the scalar mass matrix. This parametrization is useful because θ and the mass eigenvalues M_{h_1}, M_{h_2} are experimentally more accessible than the Lagrangian parameters in (5.1). In the limit $b_1, a_1, b_3 \to 0$, the theory admits a Z_2 symmetry under $S \to -S$, and the mixing vanishes. The Z_2-symmetric model has a number of interesting applications in cosmology, see *e.g.* [141, 142].

The model is constrained experimentally by EW precision measurements and direct searches for weakly-interacting states; detailed discussions appear in [143, 144]. For $\sin\theta \approx 0$, the singlet-like eigenstate couples to the SM only through the Higgs, and prospects for detection at colliders are slim [57]. However, if the theory has a first-order EWPT, one may hope to probe the model indirectly through gravitational waves. 1-loop studies of the EWPT in this model appear in [49–51, 56, 57, 59, 60, 67–71, 75–77] and references therein. The analyses suggest that a strong first-order EWPT ($v/T > 1$) can occur both in the general model (5.1) but also in its Z_2-symmetric version. Ref. [3] extended this calculation to 2-loop order and investigated the magnitude of 2-loop effects.

5.2 Thermal effective potential

Within perturbation theory, one may study phase transitions in BSM settings by means of the effective potential, V_{eff} [145]. It is the quantum analogue of the classical scalar potential, and its minimum gives the true ground state of the theory. In thermal context, the value of V_{eff} at its minimum coincides with the free energy [99]. For cosmology one is interested in strong transitions, and we may hope that the perturbative method is at least qualitatively correct if the EWPT is strongly first order, far from the second-order endpoint where the IR behavior is particularly problematic.

To calculate V_{eff}, we first introduce homogeneous background fields v and x by shifting

$$\phi \to \phi + \frac{1}{\sqrt{2}}\begin{pmatrix}0\\ v\end{pmatrix}, \qquad S \to S + x, \tag{5.4}$$

and treat these as free parameters that modify the masses and interaction vertices in the Lagrangian.[17] We work in R_ξ Landau gauge, $\xi = 0$, so that Faddeev-Popov ghosts are massless and decouple from the scalars at tree level. Counting the massive states at tree level, there are two physical scalars h_1, h_2, three "Goldstones" that, in Landau gauge, are massless in the tree-level minimum but massive for general values of v, x, and three massive vector bosons $W_\mu^\pm, Z_\mu$ as in the SM. Fermion masses are proportional to v, and to good approximation we only need the top quark t (which comes in three QCD colors).

The effective potential can obtained by integrating over all non-zero momentum modes [150]. The leading correction ("1-loop") comes from quadratic terms in the Lagrangian and can be expressed in terms of functional determinants of inverse propagators [146]. Explicitly, the effective

[17] This choice of v is obviously gauge dependent. In fact, the use of a gauge-dependent background field can lead to residual gauge dependence in the results [146]. But because the all-orders effective potential is gauge-invariant at its minima, the residual gauge-dependent corrections can be avoided by a consistent perturbative expansion [147, 148]. However, ref. [147] also discusses that because of IR divergences, this approach is not necessarily useful for the EWPT. Alternatively, a manifestly gauge-invariant effective potential can be constructed using gauge-invariant background fields [149].

potential up to 1-loop order reads

$$V_{\rm eff}(v,x) = V_0(v,x) + V_1(v,x) \tag{5.5}$$

$$V_0(v,x) = \frac{1}{2}m_\phi^2 v^2 + \frac{1}{4}\lambda v^4 + b_1 x + \frac{1}{2}m_S^2 x^2 + \frac{1}{3}b_3 x^3 + \frac{1}{4}b_4 x^4 + \frac{1}{4}a_1 x v^2 + \frac{1}{4}a_2 x^2 v^2 \tag{5.6}$$

$$V_1(v,x) = 2dJ_b(m_W^2) + dJ_b(m_Z^2) + J_b(m_{h_1}^2) + J_b(m_{h_2}^2) + 3J_b(m_G^2) - 12J_f(m_t) + \text{const}, \tag{5.7}$$

where the masses in V_1 are background-field dependent, and up to $1/\epsilon$ parts the integrals are given by [82]

$$\begin{aligned} J_b(m^2) &\equiv \frac{1}{2}\sum\!\!\!\!\!\!\int_P \ln(P^2+m^2) \\ &= -\frac{\pi^2T^4}{90} + \frac{m^2T^2}{24} - \frac{(m^2)^{3/2}T}{12\pi} - \frac{m^4}{2(4\pi)^2}\ln\left(\frac{\bar\mu e^{-\gamma_E}}{4\pi T}\right) + O\left(\frac{m^6}{\pi^4T^2}\right) \end{aligned} \tag{5.8}$$

$$\begin{aligned} J_f(m^2) &\equiv \frac{1}{2}\sum\!\!\!\!\!\!\int_{\{P\}} \ln(P^2+m^2) \\ &= \frac{7}{8}\frac{\pi^2T^4}{90} - \frac{m^2T^2}{48} - \frac{m^4}{2(4\pi)^2}\ln\left(\frac{\bar\mu e^{-\gamma_E}}{\pi T}\right) + O\left(\frac{m^6}{\pi^4T^2}\right). \end{aligned} \tag{5.9}$$

In the above, $d = 3-2\epsilon$, $\bar\mu$ is the $\overline{\rm MS}$ renormalization scale and $\gamma_E \approx 0.577$ is the Euler-Mascheroni constant. The integrals are given in high-T expansion. Accordingly, we assume that all masses are parametrically light, $m \lesssim gT$. As discussed earlier, this is typically justified near the phase transition, but can fail deep in the low-T phase if the ground-state values of v, x are large. Expressions for the field-dependent masses can be found in [3].

5.3 Resumming the potential

The bosonic sum-integral (5.8) contains a term proportional to m^3 that is non-analytic in m^2 and arises from the Matsubara zero modes. It is parametrically $O(g^3)$. However, at finite T the expression (5.7) is not the *full* $O(g^3)$ result. This is because the zero modes obtain quadratic mass corrections of order $(gT)^2$, which is of the same order of magnitude as the tree-level m^2. Thus the tree-level action is not a good starting point for perturbation theory. The solution is to *resum* the zero-mode propagators by replacing the tree-level masses with thermally-corrected ones, *i.e.* substitute $(m^2)^{3/2} \to (m^2+\Pi_T)^{3/2}$ in the zero-mode part, where Π_T denotes the thermal self-energy correction. This prescription sums the so-called thermal "daisy" diagrams to all orders of perturbation theory, correcting the $V_{\rm eff}$ at order g^3 [151, 152].

The 2-loop correction to $V_{\rm eff}$ is calculated from 1PI vacuum diagrams. These produce field-dependent terms at $O(g^4)$, meaning that the relative improvement from a resummed 1-loop calculation is only of order g. This reflects the IR sensitivity and slow convergence of finite-T perturbation theory. Furthermore, at 2-loop order the required resummations get considerably more complicated. As explained in [134], resummation at any given order of perturbation theory can be carried out by first integrating out the hard Matsubara modes, then calculating the effective potential for the remaining zero modes with modified parameters. But this is precisely the 3d

description of dimensional reduction! Indeed, by working in the 3d approximation, we automatically implement all required resummations in an easily tractable fashion. However, this clearly works only in the high-T limit and in fact, resummation becomes ambiguous at 2-loop order if there is no clear scale hierarchy between the zero and non-zero Matsubara modes. A detailed discussion of this issue appears in [82]. As before, the validity of this high-T assumption can be tested by examining the higher-order operators generated in the dimensional reduction.

With the above considerations in mind, our approach in [3] was to first dimensionally reduce the theory, then compute the effective potential in the 3d EFT to two loops. This gives the full $O(g^4)$ result for V_{eff}.[18] The full expression is too lengthy to be reproduced here, but can be read from [3]. An additional benefit of working in the 3d approach is that the renormalization group equations can be solved exactly in 3d, allowing for an efficient RG improvement of the perturbative potential [91].

5.4 Results at 2-loop order

Using the 2-loop potential, we look for temperatures where the V_{eff} admits degenerate minima with respect to the background fields. This defines the critical temperature T_c. Fig. 5.1 shows the evolution of the global minimum as a function of T, in three benchmark (BM) points (specifics can be found in the paper [3]). We also show the 1-loop plots for comparison. In the general xSM with cubic couplings, the singlet VEV is non-vanishing both in the EW "symmetric" and "broken" phases. This is adequate for strengthening the phase transition in the Higgs direction, as the background field x can produce a potential barrier already at tree level.

In contrast, a non-vanishing singlet VEV in the Z_2 symmetric model signals spontaneous breakdown of the discrete symmetry. It can happen that the singlet undergoes a symmetry-breaking transition at a high T, and the actual EWPT occurs only at a lower temperature. This is the so-called two-step EWPT scenario [46, 62], demonstrated in the (c) panel of fig. 5.1. The resulting EWPT is often very strong and therefore promising both for baryogenesis and gravitational-wave prospects. However, 1-loop parameter scans performed in [70] suggest that two-step transitions occur only in a very limited region of the parameter space. A further restriction on two-step transitions is that the rate of bubble nucleation in the second step may be too slow to overcome the expansion rate of the universe, and the EWPT never completes. We do not consider the nucleation rate here.

As the figure suggests, T_c can be quite sensitive to the 2-loop correction. This is alarming, because T_c sets the scale for other dimensionful quantities of interest and particularly the latent heat L. In [3], our 2-loop results for the dimensionless ratio L/T^4 consistently deviated from the 1-loop prediction by at least 20% and in some cases by as much as 100%. L/T^4 is the relevant measure of transition strength for gravitational-wave studies [36]. Panel (b) of fig. 5.1 further shows that a transition that looks strong at 1-loop can vanish almost completely at 2-loop order.

[18] The full xSM involves dimensionful cubic couplings a_1, b_3 and it is not obvious what power-counting scheme one should adopt for these. If the scalar masses are $m \sim gT$, then naive perturbativity requires $a_1, b_3 \sim g^2 T$, which is what we used in [3]. Different counting was adopted in [102], which also considered dimensional reduction of the xSM.

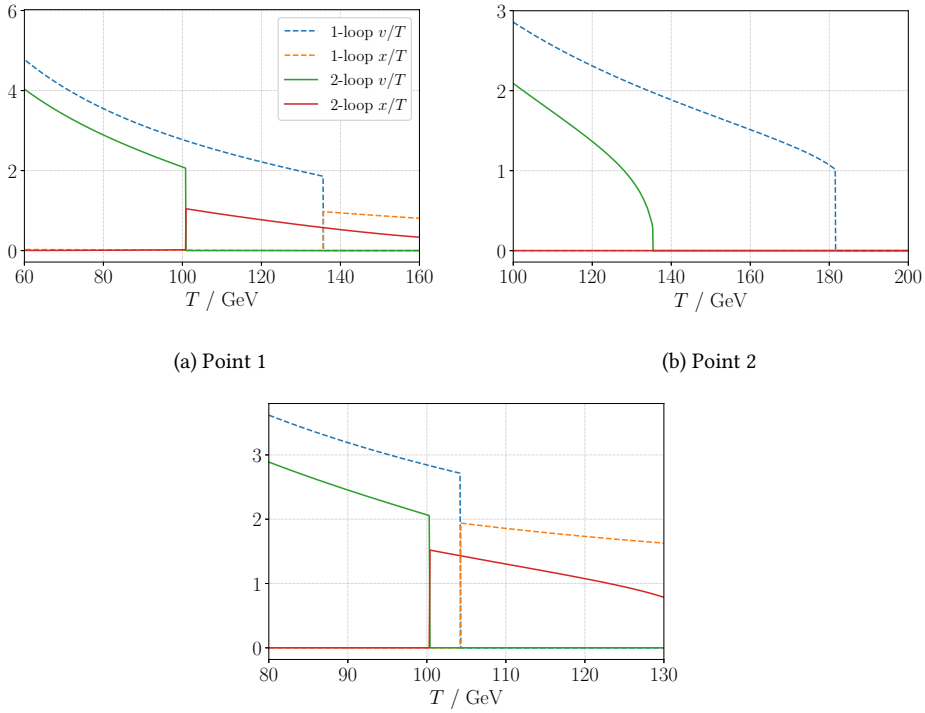

(a) Point 1

(b) Point 2

(c) Point 3

Figure 5.1: Evolution of the global minimum of $V_{\text{eff}}(v, x)$ in chosen benchmark points. Panels (a) and (b) show direct EW symmetric → broken EWPT while (c) features also spontaneous breakdown of the singlet Z_2 symmetry at a high temperature. The dashed lines correspond to 1-loop predictions.

For baryogenesis, the primary quantity of interest is the discontinuity $\Delta v/T$ of Higgs VEV across the transition.[19] Fig. 5.2 shows projections of the potential in the v direction and evaluated at T_c. In panels (a) and (c) the EWPT remains strong enough for baryogenesis at 2-loop order. Also shown is the (in)sensitivity of the 2-loop potential to variations in the RG scale, corresponding to uncanceled higher-order logarithms. The scale dependence is found to be extremely mild, except for in the Z_2 symmetric model where there is no potential barrier at tree level. Ref. [3] also studied the leading dimension five and six operators that were neglected from the 3d EFT, with the conclusion that the accuracy of dimensional reduction should be comparable to the SM case,

[19] As already discussed, v/T is, strictly speaking, not a very meaningful quantity to measure since v is gauge dependent, and the non-perturbative condition for baryogenesis is much more complicated than $\Delta v/T > 1$ (see footnote in section 4.2). We may instead look at the gauge-invariant condensate $\langle\phi^\dagger\phi\rangle/T^2$ and use its jump across the transition as a rough estimator of transition strength. This is both gauge- and RG-invariant [92], and is close to the Landau gauge value of $(\Delta v/T)^2$ [3, 82].

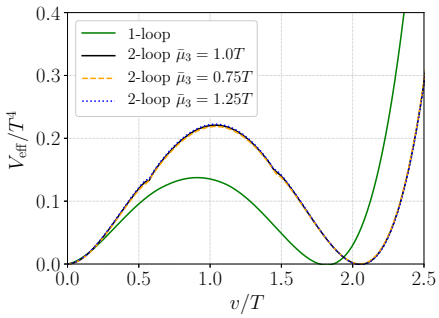

(a) Point 1

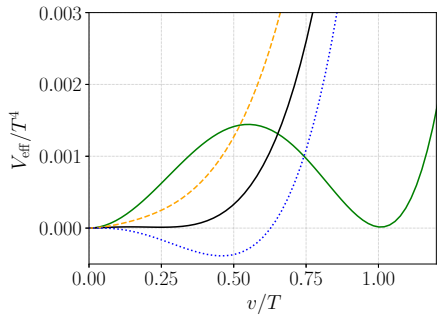

(b) Point 2

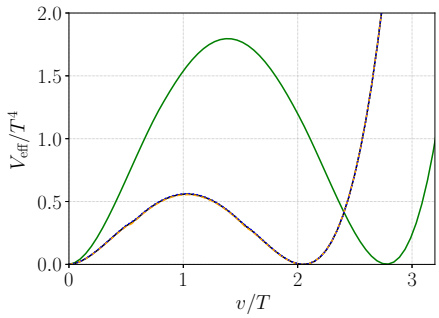

(c) Point 3

Figure 5.2: Shape of the effective potential at T_c, plotted along the Higgs direction. Residual dependence on the RG scale $\bar{\mu}_3$ is depicted by dashed and dotted lines and is non-negligible only in panel (b), where there is no potential barrier at tree level. Near the local maximum, the potential develops an imaginary part due to tachyonic scalar modes [153]. The perturbative expansion is ill-behaved at isolated points where these modes are massless, resulting in the kinks visible in panels (a) and (c).

despite the presence of relatively heavy excitations in the Higgs phase.

It should be pointed out that both the latent heat and field discontinuities should be evaluated at a supercooled temperature close to where the phase transition completes, instead of at T_c, for cosmologically relevant predictions. However, the discrepancy between 1- and 2-loop results in fig. 5.1 shows no significant improvement at lower temperatures, so it seems likely that the relative magnitude of 2-loop corrections remains roughly the same there.

5.5 Accuracy of the perturbative approach

As discussed, at finite T the system is inherently non-perturbative in the deep IR, meaning that all gauge fields are strongly coupled in the symmetric phase where $v = 0$. This is a problem,

because knowing the free energy both in the symmetric and broken regime is a pre-requisite for reliably predicting T_c and other thermodynamical parameters. By parametric counting one sees that the incalculability due to massless gauge bosons is of order g^6 and thus does not affect 2-loop results. However, there is no *a priori* reason to trust a low-order calculation if the higher-orders are non-perturbative. How accurately can we trust the 2-loop predictions?

After the EWPT, all SU(2) gauge fields have masses of order gv. Since the scale of non-perturbative physics is g^2T, one may expect the broken phase to be in perturbative control in the regime where $v \gtrsim T$, *i.e.* for strong transitions. This, however, applies only to gauge interactions, for which the high-T expansion parameter is g^2T/m_W.[20] In BSM settings such as the xSM, the EWPT is produced by scalar loops, and the relevant expansion parameter is instead $\lambda_{\rm BSM}T/m_{\rm scalar}$, where $\lambda_{\rm BSM}$ denotes a generic quartic coupling among the scalars. As discussed, the EWPT is typically associated with relatively large couplings, so there is no guarantee that ratios like this are small in the vicinity of T_c where the Higgs is parametrically light. Thus we may anticipate significant corrections at higher loop orders, and perhaps even at the non-perturbative level.

Some intuition can be drawn from non-perturbative studies in other models, particularly the SM and the Minimally Supersymmetric Standard Model (MSSM). Comparison with lattice simulations shows that deep in the symmetric or broken phases, perturbation theory is in good agreement with the non-perturbative results for quantities specific to the Higgs field, but blows up near the crossover temperature [88]. In the MSSM, the EWPT can be first order and has been studied on the lattice in [81, 154, 155]. The non-perturbative latent heat was found to differ from the 2-loop expectation by 50% in ref. [81]. We recently reported on non-perturbative results in SU(2) doublet [1] and triplet [2] extended models, where 2-loop estimates were found to agree qualitatively, but differ substantially in the quantitative values. It therefore seems likely that non-perturbative studies are required to capture the thermodynamics of the EWPT also in the xSM, and more generally in BSM theories.

It is important to emphasize that the above comparisons with lattice results were performed using 2-loop (or 3-loop as in [88]) effective potentials. On the contrary, almost all EWPT studies in BSM settings are based on 1-loop calculations [46–79], and as our analysis in the xSM demonstrates, the 2-loop correction can have a very substantial effect (see also [1, 82]). For instance, there is virtually no reason to trust gravitational-wave predictions based on 1-loop calculations if the central quantity L/T^4 changes by $\mathcal{O}(100\%)$ once 2-loop corrections are incorporated. These considerations strongly motivate improved analyses in the xSM at 2-loop, and eventually at the non-perturbative level.

[20] In the minimal SM, dominant contributions to $V_{\rm eff}$ arise from gauge loops because the Higgs self-coupling is small [134].

Chapter 6

Lattice Monte Carlo simulations of the electroweak phase transition

Non-perturbative lattice simulations are the state-of-art approach to EW thermodynamics. Ultimately, the validity of perturbative results in a high-T setting can only be addressed in a non-perturbative framework, and in this chapter we describe how the EWPT can be tackled using numerical simulations in lattice QFT. As the volume will be finite in simulations, we must specify how the fields behave at the boundaries. We will adopt periodic boundary conditions in the following, which are convenient for preserving translational invariance.

On a discrete and finite-volume lattice, all QFT expectation are nothing more than ordinary Riemann integrals over field configurations and in principle, can be evaluated using numerical integration techniques. The dimensionality of these integrals is huge, number of lattice sites times the number of field degrees of freedom. This fact renders many "standard" integrators, such as the trapezoidal rule, practically useless for the task. Instead, the go-to method is that of Monte Carlo integration, where the integral is approximated by sampling randomly-generated values for the integrand based on some probability distribution.

In our case the integrals are of the form

$$\langle O \rangle = \frac{\int [d\phi]\ O e^{-S(\phi)}}{\int [d\phi]\ e^{-S(\phi)}} = Z^{-1} \int [d\phi]\ O e^{-S(\phi)} \tag{6.1}$$

and are strongly peaked according to the "canonical" distribution $p(\phi) \sim e^{-S[\phi]}$, so the expectation values obtain dominant contributions from field configurations where the action S evaluates to a value close to its global minimum. Configurations for which the action is large provide only exponentially small corrections. Thus the numerical estimation of expectation values (6.1) using Monte Carlo necessitates *importance sampling* of field configurations: we must evaluate the integrand near its peak more frequently than elsewhere in the domain of integration. The purpose of a Monte Carlo simulation is generate field configurations according to a desired distribution.

6.1 Markov chains

A typical Monte Carlo simulation proceeds as follows. Starting from an initial field configuration ϕ_1, we modify the field variables according to some stochastic process $\mathcal{P}$ to obtain a new

configuration of fields, ϕ_2. Repeated applications of $\mathcal{P}$ produce a chain of configurations,

$$\phi_1 \overset{\mathcal{P}}{\mapsto} \phi_2 \overset{\mathcal{P}}{\mapsto} \phi_3 \overset{\mathcal{P}}{\mapsto} \phi_4 \overset{\mathcal{P}}{\mapsto} \cdots . \tag{6.2}$$

A simple choice for the process $\mathcal{P}$ is one where the transition probability $P(\phi_i \mapsto \phi_{i+1})$ depends only on the present configuration ϕ_i, and not on earlier elements in the chain. With this property, the chain (6.2) is called a *Markov chain* and $\mathcal{P}$ its associated Markov process. In computer simulations, the mapping $\phi_i \mapsto \phi_{i+1}$ is often referred to as an *update* step. Updating fields on all lattice sites is called an *update sweep*.

Suppose our transition probabilities are so that the probability distribution of ϕ_i is $p(\phi) = Z^{-1}e^{-S(\phi)}$, *i.e.* the configurations come from the canonical ensemble. If we measure a quantity $O_i = O[\phi_i]$ from each configuration, the ensemble average (6.1) can be *estimated* by

$$\bar{O}_N = \frac{1}{N}\sum_{i=1}^{N} O_i. \tag{6.3}$$

We will refer to the set of measurements O_i as a *sample* and $\bar{O}_N$ is the *sample mean*, which coincides with the ensemble average $\langle O \rangle$ for $N \to \infty$. The sample mean can be thought of as a random variable fluctuating around $\langle O \rangle$. From the central limit theorem it follows that for large N, the distribution of $\bar{O}_N$ tends to a Gaussian if all measurements are statistically independent, with variance $\sigma_N^2 = s^2/N$. The coefficient s^2 is simply the variance of the measurements O_i (*sample variance*). In reality the measurements are often correlated and the error estimate is more involved. This is discussed in Section 6.2 below.

How should the probabilities $P(\phi_i \mapsto \phi_{i+1})$ be chosen in order to achieve the equilibrium distribution $p_{\text{eq}}(\phi) \propto e^{-S}$? It is important to realize that the probability distribution need not remain unchanged at different stages of the Markov chain. In fact, applying $\mathcal{P}$ to all configurations in the ensemble shows that the distribution changes as

$$p_i(\phi_i) \mapsto p_{i+1}(\phi_{i+1}) \equiv \int d\phi \; p_i(\phi) P(\phi \mapsto \phi_{i+1}), \tag{6.4}$$

and we denote $p_i(\phi_i) \overset{\mathcal{P}}{\mapsto} p_{i+1}(\phi_{i+1})$. We will make two intuitive assumptions about the Markov process $\mathcal{P}$:

1. The equilibrium distribution is a fixed point of $\mathcal{P}$, $p_{\text{eq}}(\phi_i) \overset{\mathcal{P}}{\mapsto} p_{\text{eq}}(\phi_{i+1})$.

2. The process $\mathcal{P}$ is *ergodic*: Any field configuration is accessible from an arbitrary initial configuration by a repeated application of $\mathcal{P}$.

Ergodicity guarantees that the fixed point is unique. Remarkably, the fixed point is also a limiting distribution of the Markov chain. In other words, starting from *any* initial configuration ϕ_i and repeatedly applying $\mathcal{P}$ will get us arbitrarily close to the equilibrium distribution. A proof of these properties can be found in [156].

6.2 Autocorrelation and statistical errors

The reliability of Monte Carlo integration hinges on our ability to obtain statistically independent measurements of a given quantity. But subsequent configurations generated by a Markov process are not necessarily uncorrelated, as often the new configuration is just a small modification of the old one. Thus it is crucial to estimate the statistical errors associated with our Monte Carlo results. A proper mathematical treatment of the uncertainty associated with correlated measurements requires careful *time series analysis* (time series in this case being the measurements O_i associated with a Markov chain). Here we give just a practical overview of the main results.

The correlation of measurements O_i is described by the *autocorrelation* function,

$$\begin{aligned} C_O(t) &= \langle O_i O_{i+t}\rangle - \langle O_i\rangle\langle O_{i+t}\rangle = \langle O_i O_{i+t}\rangle - \langle O\rangle^2 \\ &= \Big\langle \big(O_i - \langle O\rangle\big)\big(O_{i+t} - \langle O\rangle\big)\Big\rangle, \end{aligned} \tag{6.5}$$

where $\langle\cdot\rangle$ refers to the expectation value of infinitely many measurements. In the language of statistics, autocorrelation is the covariance of random variables O_i and O_{i+t}. We also define the normalized autocorrelation function $\rho_O(t) = C_O(t)/C_O(0)$, which decays exponentially for typical observables [157],

$$\rho_O(t) \sim e^{-|t|/\tau} \quad \text{for large } t. \tag{6.6}$$

The decay of autocorrelation is characterized by the *exponential autocorrelation time* τ_{exp} ("time" here refers to the simulation time labeling configurations or measurements). In principle, different observables can exhibit different autocorrelations, and τ_{exp} is usually defined as the relaxation time of the slowest mode in the system, formally

$$\tau_{\text{exp}} = \sup_O \lim_{t\to\infty} \frac{t}{-\ln|\rho_O(t)|}. \tag{6.7}$$

The exponential autocorrelation time is a measure of when field configurations generated by the Markov process become thoroughly uncorrelated. In fact, τ_{exp} is also the characteristic time scale needed to reach the equilibrium distribution from a given non-equilibrium configuration [158].

We can write the variance σ_N^2 of the sample mean in terms of the autocorrelation function:

$$\begin{aligned} \sigma_N^2 &= \Big\langle (\bar{O}_N - \langle O\rangle)^2 \Big\rangle = \Big\langle \frac{1}{N^2}\sum_{i,j=1}^{N} \big(O_i - \langle O\rangle\big)\big(O_j - \langle O\rangle\big)\Big\rangle \\ &= \frac{1}{N^2}\sum_{i,j=1}^{N} C_O(i-j) = \frac{1}{N}\sum_{t=-(N-1)}^{N-1}\left(1 - \frac{|t|}{N}\right) C_O(t) \end{aligned} \tag{6.8}$$

where the last equality is a summation identity. For large $N \gg \tau_{\text{exp}}$, the variance behaves as

$$\sigma_N^2 \xrightarrow{N\to\infty} C_O(0)\frac{2\tau_{\text{int},O}}{N}, \tag{6.9}$$

where the *integrated autocorrelation time* associated with O is defined as

$$\tau_{\text{int},O} = \frac{1}{2}\sum_{t=-\infty}^{\infty} \rho_O(t)\left(1 - \frac{|t|}{N}\right). \tag{6.10}$$

The subleading term $|t|/N$ is often dropped in the literature, and the conventional factor $1/2$ ensures that $\tau_{\mathrm{int},O} \approx \tau_{\mathrm{exp}}$ if the normalized autocorrelation function is purely exponential [157]. Because $C_O(0)$ is simply the variance of O_i, we see that the true variance of $\bar{O}_N$ in the presence of autocorrelations is $2\tau_{\mathrm{int},O}$ times larger than if the measurements were uncorrelated. In other words, there are effectively $N/(2\tau_{\mathrm{int,O}})$ independent measurements of O. The error of a Monte Carlo average is typically given as a one-σ error.

In real applications, our sample O_i is finite (size N) and the autocorrelation needs to be estimated accordingly. There are $N - |t|$ measurements of $O_i O_{i+t}$, so a natural estimator of (6.5) is

$$\bar{C}_O(t) \approx \frac{1}{N-|t|} \sum_{i=1}^{N-|t|} O_i O_{i+t} - \bar{O}_i \bar{O}_{i+t} \tag{6.11}$$

where we defined

$$\bar{O}_i = \frac{1}{N-|t|} \sum_{i=1}^{N-|t|} O_i, \qquad \bar{O}_{i+t} = \frac{1}{N-|t|} \sum_{i=1}^{N-|t|} O_{i+t}. \tag{6.12}$$

To calculate the integrated autocorrelation time from a finite sample, we first note that the "natural" estimate of (6.10),

$$\tau_{\mathrm{int},O}^{(\mathrm{naive})} = \frac{1}{2} \sum_{t=-(N-1)}^{N-1} \frac{\bar{C}_O(t)}{\bar{C}_O(0)} \frac{N-|t|}{N} \tag{6.13}$$

is extremely noisy for $|t| \gg \tau_{\mathrm{exp}}$ because the signal falls off exponentially. A better estimator is obtained by truncating the sum to values $|t| < M$, *e.g.*

$$\bar{\tau}_{\mathrm{int},O} = \frac{1}{2} \sum_{|t|<M} \frac{\bar{C}_O(t)}{\bar{C}_O(0)} \frac{N-|t|}{N} = \frac{1}{2} + \sum_{t=1}^{M} \frac{\bar{C}_O(t)}{\bar{C}_O(0)} \frac{N-t}{N}, \tag{6.14}$$

and M is chosen to retain most of the signal while discarding the noise. We assumed invariance under time translations in the above, which obviously holds in equilibrium.

Assuming $\tau_{\mathrm{exp}} \ll M \ll N$, this estimator has variance

$$\sigma^2_{\bar{\tau}_{\mathrm{int},O}} \approx \frac{2(2M+1)}{N} \tau^2_{\mathrm{int},O}, \tag{6.15}$$

and the cutoff M introduces a bias of order $1/N$ [159]. Thus a good choice of M is one that provides reasonable balance between bias and variance. In practice, we use a "self-consistent" value of $M = 6\bar{\tau}_{\mathrm{int},O}$. Ideally, if $\rho(t)$ were a pure exponential this would lead to an error of order $e^{-6} \approx 10^{-3}$. This procedure is known to work well at least for large data sets ($N \gtrsim 1000\tau_{\mathrm{int},O}$) [157].

In addition to ensemble averages $\langle O \rangle$, we will often want to calculate functions of the type $f(\langle O \rangle)$. The Monte Carlo estimate is naturally $f(\bar{O}_N)$, but the above analysis is not suitable for calculating the error δf for non-linear functions. A convenient way to compute the statistical uncertainty of $f(\bar{O}_N)$ is through standard *jackknife* analysis; we refer to [160] for details. In this thesis and associated publications, statistical errors of "primary" quantities like $\bar{O}_N$ are estimated based on the integrated autocorrelation times (6.14), while for "secondary" quantities (functions like $f(\bar{O}_N)$) we apply the jackknife method. In fact, the jackknife and related resampling techniques could be used to estimate τ_{int} as well, see e.g. [161].

6.3 Implementing field update algorithms

It remains to construct an explicit field update algorithm that is ergodic and has p_{eq} as its fixed point. The distribution of field configurations produced by any such algorithm will tend to the canonical one irrespectively of how the starting configuration was chosen; we say that the system *thermalizes* to equilibrium on a time scale of order τ_{exp}. The magnitude of autocorrelations naturally depends on details of the chosen algorithm.

Often one considers updates that are reversible at the microscopic level,

$$P(\phi \mapsto \phi')p_{\text{eq}}(\phi) = P(\phi' \mapsto \phi)p_{\text{eq}}(\phi'), \tag{6.16}$$

as it is easy to show that p_{eq} is a fixed point of such an update. The condition (6.16) is called *detailed balance*. One of the most common updates is the Metropolis algorithm [162], defined (up to a normalization) by

$$P(\phi \mapsto \phi') = \begin{cases} e^{-\delta S} & \text{if } \delta S > 0 \\ 1 & \text{otherwise,} \end{cases} \tag{6.17}$$

where $\delta S = S(\phi') - S(\phi)$ is the change in the action. This update is obviously ergodic and satisfies detailed balance, so its limiting distribution is the canonical one. The Metropolis update depends only on the difference δS, which is readily calculable in a typical simulation program. Hence, the Metropolis algorithm can be applied to almost any system.

For many systems (those describable in terms of local Lagrangians), the Metropolis update can be implemented as a *local* operation: The change δS due to a field update at point x can be calculated using only fields at point x and its nearest neighbors, and the fields can be updated in a site-by-site fashion. A simple implementation of the local Metropolis update is the following (for concreteness, take ϕ to be a real scalar):

1. Choose a lattice site x and evaluate $S_x(\phi)$, the contribution to the action due to ϕ at site x.
2. Pull a (pseudo-)random number X from a uniform distribution, $X \in [0, 1]$. Choose new $\phi'_x = \phi_x + C(X - 0.5)$, where C is a tunable constant.
3. Evaluate the local change in the action, $\delta S_x = S_x(\phi') - S_x(\phi)$, and accept the update with probability $\min(e^{-\delta S_x}, 1)$. If rejected, keep the old value ϕ_x.

A Metropolis update sweep consists of steps 1. through 3. applied once to all sites on the lattice.

Because local field updates at neighboring sites are generally not independent, one needs to make sure that the ordering of updates is consistent with ergodicity and detailed balance. All simulations in this thesis use a "checkerboard" ordering, where we associate a parity label to each lattice site. A site has even (odd) parity if the sum of its coordinates $(x_1, x_2, \dots)$ is even (odd), and the update sweep is carried out by first performing local updates on all even sites, followed by local updates on odd sites. Since there are only nearest-neighbor interactions, the checkerboard ordering guarantees that the odd sites are updated independently of even sites.

It is also possible to perform the update *globally*, *i.e.* simultaneously on all sites, but local algorithms are usually more efficient. This is because global updates to fields are more likely to

move the system out of equilibrium and are thus prone to high rejection rates, unless the fields are changed only slightly, which in turn requires many update sweeps to produce statistically independent configurations. The acceptance rate of the Metropolis update can be adjusted by tuning the constant C, and a rate of $\sim 50\%$ is typically suitable.

A plethora of more model dependent update algorithms exist in the literature. Many of these are optimized to reduce autocorrelations more effectively than the Metropolis update, while still exhibiting high acceptance rates. We mention in particular the SU(2) heatbath algorithm of ref. [163] and the Higgs overrelaxation update described in [85, 154]. Both of these can be applied locally and generalize easily to the BSM context. The update sweep used in simulations described in this thesis consists of a heatbath update of the gauge links, followed by five overrelaxation and one Metropolis update of the scalars. The Metropolis step is needed because the overrelaxation update by itself is not ergodic.

6.4 First-order transitions in simulations

Once our simulation has accumulated many measurements of some quantity O_i, it is often interesting to look not only at the sample mean $\bar{O}$, but also the distribution of the measurements (*i.e.* the histogram). It corresponds to the actual probability distribution of the quantity, provided that the simulation is able to probe the whole ensemble of configurations without *e.g.* getting stuck in one region of the configuration space due to a strong energy barrier. Such barriers actually complicate simulations of first-order phase transitions, and an algorithm designed for overcoming these difficulties is described in section 6.5 below.

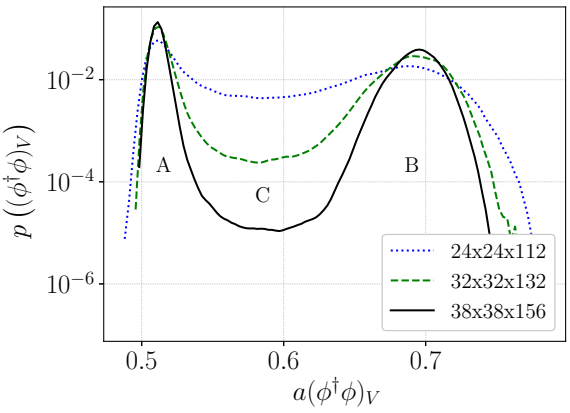

Figure 6.1: Sample histograms at different volumes for the volume average of $\phi^\dagger\phi$ (in natural lattice units). Regions A and B correspond to pure-phase field configurations and C to mixed-phase configurations, as described in the text. Data is from the simulations discussed in section 7.2.

In first-order transitions we are particularly interested in order-parameter like quantities that are discontinuous[21] across the phase boundary, for instance the gauge-invariant expectation value $\langle\phi^\dagger\phi\rangle$. Let us define the *volume average* of a local quantity O as the mean across all N_s lattice sites,

$$(O)_V \equiv \frac{1}{N_s}\sum_x O(x). \tag{6.18}$$

Near the critical temperature, the distributions of such quantities have a characteristic two-peak structure.[22] A sample distribution of $(\phi^\dagger\phi)_V$ at different volumes is shown in fig. 6.1. We follow [140] in discussing its properties.

Configurations where the quantity $\phi^\dagger\phi$ evaluates to a value within the peak A or B are those where the entire lattice is "in one phase", in the sense that the coarse-grained quantity $\phi^\dagger\phi$ is spatially homogeneous. The peaks A and B are the "pure" or "bulk" phases. More specifically, the composite operator $\phi^\dagger\phi$ is UV divergent and fluctuates from point to point, but the coarse-grained operator obtained by averaging over distances longer than the bulk correlation length is approximately homogeneous. In the SM case, the peak A at smaller values of $(\phi^\dagger\phi)_V$ corresponds to the EW-symmetric phase and peak B is the broken Higgs phase. At the critical temperature T_c, it is equally probable the find the system in either of the phases. In contrast, configurations for which the volume average $(\phi^\dagger\phi)_V$ lies in between the peaks are exponentially rare: region C in the figure. This is essentially the statement that the phases A and B are separated by a first-order transition. Thus to find T_c, we look for a temperature where the integrated areas of A and B are equal.[23] Note that because configurations in region C are suppressed, it is exponentially unimportant how the separation point between A and B is chosen.

Crucially, the exponential suppression of configurations in region C increases with growing lattice volume, as shown in the figure. Naively, this is because the free-energy cost of configurations, in which (the coarse-grained) $\phi^\dagger\phi$ is homogeneous and far from the equilibrium value, scales extensively with the volume. But it costs less free energy to form inhomogeneous configurations where part of the volume is in phase A and the other part in phase B, so that $(\phi^\dagger\phi)_V$ takes a value in region C. For these "mixed" configurations the disfavored values of $\phi^\dagger\phi$ appear only in the interface separating the phases, so the free-energy cost scales instead with the interface area. Thus the majority of configurations in region C are actually inhomogeneous mixed-phase configurations.

6.5 Multicanonical algorithm for first-order transitions

The exponential suppression of mixed-phase configurations means that common simulation algorithms sampling configurations in the canonical ensemble will very rarely end up in region C of the probability distribution in fig. 6.1. In practice, on large lattices the simulation will thermalize to either phase A or B and remain stuck there for a very long time, as an exponentially rare

[21] Strictly speaking, there are no phase transitions in a finite system, and the order parameters are only "almost" discontinuous as is evident from fig. 6.1. There is no ambiguity in stating that a true phase transition exists if the almost discontinuous behavior persists, and grows stronger, as the volume is increased indefinitely.

[22] At a triple point there would be three peaks, and so on.

[23] This is the "equal weight" criterion for T_c. Different criteria were considered in ref. [85], all of which agree on large lattices within small statistical errors.

fluctuation is needed to start the "tunneling" process. However, to determine the critical temperature we must compare the statistical weights of both phases, and it is crucial that the simulation can probe the entire range of order parameter values. Clearly, sampling algorithms based on the canonical ensemble are inadequate for simulating first-order transitions.

The standard solution to the problem is to apply *multicanonical* simulations [164, 165]. Suppose O is an order-parameter like observable that can distinguish between the different phases. The multicanonical method modifies the ensemble by a suitable weight function $W(O)$, so that the probability of mixed-phase configurations is enhanced. The distributions change as

$$p_{\mathrm{can}}(O) \propto e^{-S} \to p_{\mathrm{multi}}(O) \propto e^{-S-W(O)} \propto p_{\mathrm{can}} e^{-W(O)}. \tag{6.19}$$

Ideally, one would choose W so that the distribution is flat everywhere in the range of interest, as then the simulation would freely probe the entire configuration space in a random-walk fashion. But this ideal choice corresponds to $W(O) = \ln p_{\mathrm{can}}(O)$, which is the unknown quantity we want to obtain! Thus we must approximate W by a function that is close to the canonical distribution and allows for efficient tunneling between the bulk phases.

Recursive algorithms for approximating p_{can} have been introduced for instance in [85, 154, 164, 166]. For the simulations in this thesis we use a minor modification of the method of [166]. The field update algorithm must also be modified to sample configurations according to p_{multi} instead of the canonical distribution. However, the weight is typically a function of some global quantity (for example the volume average $(\phi^\dagger\phi)_V$), and calculating W multiple times in an update sweep can be costly. The multicanonical simulation can be optimized by performing the local updates using standard canonical algorithms, then accounting for the weight function by a global Metropolis acceptance step.

Measurements from a multicanonical simulation are distributed according to p_{multi}, but ultimately we are interested in distributions with respect to the more physical canonical ensemble. Once the weight function has been fixed, we may simply invert (6.19) to get $p_{\mathrm{can}}(O) \propto p_{\mathrm{multi}}(O)e^{W(O)}$. This is an example of the more general *reweighting* technique described in [167]. We may apply reweighting also to individual measurements O_i produced by the multicanonical simulation. The canonical Monte Carlo expectation value is then obtained as [85]

$$\bar{O}_N^{\mathrm{can}} = \frac{\sum_{i=1}^N O_i e^{W(O_i)}}{\sum_{i=1}^N e^{W(O_i)}}. \tag{6.20}$$

Apart from small-volume runs, all simulation results for first-order transitions presented in this thesis utilize the multicanonical method.

6.6 Thermodynamical parameters from the simulations

A number of thermodynamical observables can be extracted from the two-peak histogram. We already described the criterion for T_c, and let us next discuss the latent heat L. By definition, it is the energy density difference between the low- and high-T phases:

$$L = \frac{1}{V} Z^{-1} \Delta \left(\mathrm{Tr}\, H e^{-H/T} \right) = \frac{T^2}{V} \Delta \left(\frac{d}{dT} \ln Z \right) = \Delta f - T \frac{d\Delta f}{dT}, \tag{6.21}$$

where f is the free-energy density, $f = F/V$. However, from the 3d point of view there is no explicit temperature in the simulations; the theory is purely spatial and T appears only in definitions of the parameters. Instead of f, the appropriate quantity is thus the vacuum energy density of the 3d EFT,

$$\epsilon_3 = -\frac{1}{V} \ln Z, \tag{6.22}$$

which is related to the free-energy density as $f = T\epsilon_3$, plus a "cosmological constant" (as in Eq. (2.14)) that is irrelevant for phase transitions.

The vacuum energy is a function of the parameters appearing in the action, *e.g.* $\epsilon_3 = \epsilon_3(m_3^2, g_3^2, \lambda_3, a)$ for a lattice-regulated version of the EFT in eq. (4.14) (ignoring the $\mathrm{U}(1)_Y$ coupling for brevity). Its derivatives generate correlation functions of local operators, or *condensates*, that constitute the action [92]:

$$\frac{\partial \epsilon_3}{\partial \bar{m}_3^2} = \langle \phi^\dagger \phi \rangle, \qquad \frac{\partial \epsilon_3}{\partial \bar{\lambda}_3} = \langle (\phi^\dagger \phi)^2 \rangle, \tag{6.23}$$

and so on. Using ϵ_3, the latent heat can be expressed in a convenient form:

$$\frac{L}{T^4} = \frac{1}{T^2} \frac{d(\Delta\epsilon_3)}{dT} = \frac{1}{T^2} \left(\frac{d\bar{m}_2^3}{dT} \Delta\langle \phi^\dagger \phi \rangle + \frac{d\bar{\lambda}_3}{dT} \Delta\langle (\phi^\dagger \phi)^2 \rangle + \cdots \right), \tag{6.24}$$

where the ellipsis refer to other operators in the action. Generalization to BSM theories is straightforward. Thus to determine L, we must measure jumps of various local expectation values across the transition, and these are readily obtained from the histograms. The condensates by themselves are unphysical as their values depend on the renormalization point, but because the renormalization is additive the jumps in eq. (6.24) are RG invariant [92]. The quantity $\Delta\phi^\dagger\phi$ is also relevant for estimating the suppression of sphaleron transitions in the broken phase [139].

Another quantity for characterizing the transition strength is the interface tension σ of the phase boundary. It has practical use in estimating the bubble nucleation rate in the "thin-wall" approximation [168]. The interface carries free energy $F_{\mathrm{interface}} = \sigma A$, if A is the interface area, and we may utilize the inhomogeneous configurations in region C of the histogram to measure the tension σ. At large volumes, the suppression mixed-phase configurations is almost solely due to the interface tension and is proportional to $\exp(-\sigma A/T)$.

From the histogram we can measure the probability of finding the system in a mixed configuration relative to the probability of a bulk configuration in phase A (or B, since $P_A = P_B$ at T_c). Thus, the interface tension is given by [169]

$$\frac{\sigma}{T} = -\frac{1}{2A} \ln \frac{P_C}{P_A}, \tag{6.25}$$

up to corrections that vanish at $V \to \infty$. The factor of 2 appears because on a periodic lattice, there are actually two interfaces. A practical way of measuring this is to make the lattice long in, say, the z-direction, so that $L_x = L_y \ll L_z$, in which case the free energy due to a phase boundary is minimized if the interface forms perpendicular to the z-axis. For very long lattices, the histogram becomes flat in the region between bulk phases [140]. The formula (6.25) can be optimized by finite-size analysis as described in [170].

Chapter 7

Non-perturbative results in selected models

This chapter summarizes the key findings in associated publications [1] and [2], where we performed lattice studies of strong EWPT in two different models. The basic pipeline in both publications consists of high-T dimensional reduction of the BSM model onto an effective 3d theory, which is then simulated on the lattice. Simulations are used to obtain a realistic picture of the EWPT in these models and to benchmark the performance of perturbation theory. The results back up the discussion of section 5.5 that higher-order effects are indeed significant in typical BSM scenarios.

7.1 Dimensionally-reduced theories on the lattice

High-T perturbation theory is unreliable at distances $\ll 1/T$ due to long-wavelength bosons. Conversely, at energy scales $\sim \pi T$ there is no obstacle to applying perturbative methods, and we may always dimensionally reduce a given BSM model in the high-T limit if the underlying $T = 0$ theory is weakly coupled. Thus the study of BSM thermodynamics separates into two independent steps: perturbative dimensional reduction of the finite-T theory, and non-perturbative lattice simulations carried out in the 3d EFT.

But why not simply simulate the full 4d theory directly? There are several reasons why the 3d approach is both more efficient and often also more accurate [92]:

- Any realistic extension of the EW theory necessarily contains chirally-coupled fermions, for which no satisfactory lattice formulation exists as of date [118]. The top quark in particular has a significant "renormalizing" effect on the long-distance coefficients in the Higgs potential (*c.f.* equation (4.8)), and neglecting it does not seem a viable option for precision studies of the EWPT.

- Dimensional reduction removes excitations at the hard scale πT from the spectrum, making it possible to use coarser lattices than in 4d simulations without cutting out important physics at scales $\gtrsim \pi T$. Thus it is easier to simultaneously fit both short- and long-wavelength modes on the lattice by first integrating out the hard scale.

- It is substantially easier to make connection with continuum physics in 3d than in 4d. This is because often the dimensionally-reduced theory can be truncated to super-renormalizable operators, making it possible to obtain *exact* lattice-continuum relations with analytical methods [171, 172]. This point is discussed in more detail below.

There is also the obvious numerical cost associated with one extra dimension in 4d simulations. For these reasons, state-of-art simulations of the EWPT mostly utilize the 3d approach. Direct finite-T simulations in 4d exist for the SU(2) + Higgs system [8, 173, 174] and for a supersymmetric extension [175], but generally feature larger statistical and systematical errors than the 3d counterparts [85, 154, 155]. Nevertheless, the fact that (bosonic) 4d and 3d simulations agree within statistical errors strongly suggests that the perturbative dimensional reduction for hard Matsubara modes is a perfectly valid procedure.

In section 3.3 we described how to formulate gauge theories on the lattice. Following the discussion there, we may immediately write down a lattice action corresponding to the dimensionally-reduced SM:

$$\begin{aligned} S_{\text{lat}} = \beta_G \sum_{x,\, i<j} \left[1 - \frac{1}{2} \operatorname{Re} \operatorname{Tr} P_{ij}(x) \right] + 2a \sum_{x,\, i} \left[\phi^\dagger \phi - \operatorname{Re} \phi^\dagger(x) U_i(x) \phi(x+i) \right] \\ + a^3 \sum_x \left[\bar{m}_L^2 \phi^\dagger \phi + \bar{\lambda}_3 (\phi^\dagger \phi)^2 \right] \end{aligned} \tag{7.1}$$

where $\beta_G = 4/(\bar{g}_3^2 a)$ and P_{ij} is the SU(2) Wilson plaquette from (3.15). Apart from the hypercharge $\mathrm{U}(1)_Y$ content, this action reduces to eq. (4.14) in the continuum limit. Non-perturbative effects related to the hypercharge field are known to be small, affecting the transition strength by less than 10% [86]. Thus, to good approximation we may drop it from the lattice action to simplify the simulations. In practice, the lattice spacing is fixed by specifying the dimensionless β_G and the 3d gauge coupling $\bar{g}_3^2$, which follows from dimensional reduction.

All parameters appearing in the lattice action (7.1) are the unrenormalized (bare) ones. However, this theory is super-renormalizable and in particular the couplings $\bar{\lambda}_3, \bar{g}_3^2$ suffer no logarithmic divergences; up to $O(a)$ corrections they are equal to the couplings of the continuum theory. But the same is not true for the mass parameter $\bar{m}_L^2$, which is formally infinite if the UV cutoff is removed. But as physical predictions must not depend on the cutoff a, we must specify a renormalization condition that fixes $\bar{m}_L^2$ at a given lattice spacing while preserving the physics at distances $\gg a$. In principle we could proceed by calculating (non-perturbatively) some physical quantity, *e.g.* the mass of a Higgs excitation, at different spacings, and adjust $\bar{m}_L^2$ so that the result remains the same.

Fortunately, there is a better way of fixing the lattice mass parameter. From dimensional reduction we obtain the corresponding continuum parameter $\bar{m}_3^2$ in some renormalization scheme, usually $\overline{\text{MS}}$. The problem is then to find a counterterm on the lattice side such that the theories have the same IR behavior, and $\bar{m}_L^2 = \bar{m}_3^2 + \delta\bar{m}_L^2$. Because of super-renormalizability, mass divergences appear only up to a finite order of perturbation theory. By simple dimensional analysis, the mass has a linear divergence at 1-loop and logarithmic divergence at 2-loop, and at higher orders the corrections are $O(a)$. Thus we may fix the counterterm exactly, up to terms that vanish

in the continuum limit, by computing a physical quantity at 2-loop level.[24] This has been done in [171, 172] for a variety of 3d theories using the effective potential, whose minimum determines the physical equation of state. Thus the lattice results can very effectively be related to continuum physics within the 3d framework.[25] This can be contrasted to the situation in the renormalizable 4d theory, where a separate renormalization condition is required for each parameter in the action, and no analytical all-orders relations exist between the lattice and continuum parameters.

7.2 Electroweak phase transition with two Higgs doublets

In paper [1], we investigated the EWPT in the two-Higgs-doublet model (2HDM), which is a minimalistic extension of the SM containing two SU(2) scalar doublets with hypercharge $\frac{1}{2}$. The Higgs potential of this theory reads

$$\begin{aligned} V(\phi_1,\phi_2) = {} & \mu_{11}^2\phi_1^\dagger\phi_1 + \mu_{22}^2\phi_2^\dagger\phi_2 + \mu_{12}^2\left[\phi_1^\dagger\phi_2 + h.c.\right] + \lambda_1(\phi_1^\dagger\phi_1)^2 + \lambda_2(\phi_2^\dagger\phi_2)^2 \\ & + \lambda_3(\phi_1^\dagger\phi_1)(\phi_2^\dagger\phi_2) + \lambda_4(\phi_1^\dagger\phi_2)(\phi_2^\dagger\phi_1) + \frac{\lambda_5}{2}\left[(\phi_1^\dagger\phi_2)^2 + h.c.\right] \end{aligned} \tag{7.2}$$

where we restricted λ_5 and μ_{12}^2 to be real, and have dropped the so-called hard Z_2-violating operators $(\phi_1^\dagger\phi_1)(\phi_1^\dagger\phi_2)$ and $(\phi_2^\dagger\phi_2)(\phi_1^\dagger\phi_2)$. We further assume a Type-I alignment of Yukawa interactions, in which only the doublet ϕ_2 couples to the fermions. This avoids flavor-changing neutral currents at tree level [179], which are severely constrained by experiment. Thus we identify ϕ_2 as the more SM-like doublet in the following. The parameters in (7.2) are fixed by giving as inputs the pole masses of the BSM scalars and two mixing angles, *c.f.* [1] for details. A comprehensive review of two-Higgs-doublet models appears in [180].

Prospects for strong EWPT in the 2HDM have been investigated at 1-loop level in [47, 48, 52, 55, 58, 61, 64–66, 72, 73, 78, 79] and at 2-loop in [82]. Two-Higgs-doublet potentials appear also in supersymmetric extensions of the SM and the associated phase transition has been studied non-perturbatively in [155, 175]. However, the results of supersymmetric models are not directly applicable to the more minimal model in (7.2) as the explored range of parameters is very different. For instance, supersymmetry restricts all of the couplings λ_i to be small, while very strong transitions can appear in the model defined by (7.2) if the couplings are allowed to take $O(1)$ values [52, 55, 58, 61, 64, 65, 72, 78, 79, 82]. Given that such large couplings may invalidate perturbative methods even without IR issues at finite temperature [181], it is important to investigate the strong-EWPT scenario in the 2HDM also at the non-perturbative level.

Dimensional reduction for the 2HDM was worked out to full order g^4, λ_i^2 accuracy in [95]. In

[24] There is no issue in solving the counterterm using perturbation theory because strong-coupling effects appear only in the IR.

[25] It is also possible, but highly non-trivial, to derive improved relations so that the error becomes $O(a^2)$, see [176–178].

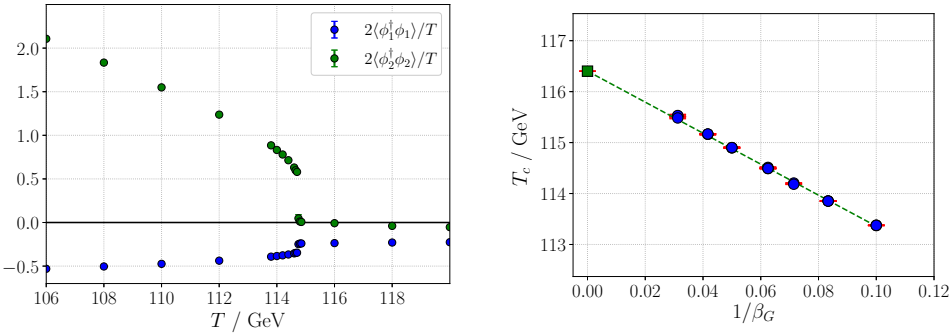

(a) (b)

Figure 7.1: Left: Non-perturbative scalar condensates in 3d, converted to $\overline{\text{MS}}$ scheme using relations given in [172] (the condensates can become negative because of the additive renormalization). The discontinuity around $T \approx 115$ GeV signals a first-order phase transition. Data are from a 48^3 lattice with $\beta_G = 4/(\bar{g}^2 a) = 16$, and statistical errors are too small to be visible at this scale. Right: Continuum extrapolation of the critical temperature. Results for T_c from different volumes fall almost on top of each other.

lattice formulation, the 3d EFT reads

$$\begin{aligned} S_{\text{2HDM}}^{(3d)} = S_W - 2a \sum_{x,i} \text{Re}\left[\phi_1^\dagger(x) U_i(x) \phi_1(x+i) + \phi_2^\dagger(x) U_i(x) \phi_2(x+i)\right] \\ + \sum_x a^3 \Big[\left(\frac{6}{a^2} + \bar{m}_{11}^2\right) \phi_1^\dagger\phi_1 + \left(\frac{6}{a^2} + \bar{m}_{22}^2\right) \phi_2^\dagger\phi_2 + \bar{m}_{12}^2 \left(\phi_1^\dagger\phi_2 + \phi_2^\dagger\phi_1\right) \\ + \bar{\lambda}_1 (\phi_1^\dagger\phi_1)^2 + \bar{\lambda}_2 (\phi_2^\dagger\phi_2)^2 + \bar{\lambda}_3 (\phi_1^\dagger\phi_1)(\phi_2^\dagger\phi_2) + \bar{\lambda}_4 (\phi_1^\dagger\phi_2)(\phi_2^\dagger\phi_1) \\ + \frac{\bar{\lambda}_5}{2} \left((\phi_1^\dagger\phi_2)^2 + (\phi_2^\dagger\phi_1)^2\right) \Big], \end{aligned} \tag{7.3}$$

where S_W is the Wilson gauge action akin to (7.1) and we neglect the hypercharge interaction. The mass parameters appearing in (7.3) are the unrenormalized ones, and their relations to continuum $\overline{\text{MS}}$ parameters are given in [155].

Panel (a) of fig. 7.1 shows the evolution of quadratic scalar condensates (in 3d units, so that $\phi^\dagger\phi/T$ is dimensionless) as function of T, measured in the global probability maximum in one benchmark point. The input parameters are given in [1]. According to perturbation theory, this point admits a strong transition with $v/T_c \approx 1.5$ at 1-loop [61] and a somewhat weaker transition ($v/T_c \approx 1$) at 2-loop [82]. A first-order transition is clearly visible also in the lattice result shown in fig. 7.1; however, this is at fixed volume and lattice spacing, and does not necessarily reflect the continuum theory in infinite volume. To quantify these finite-size effects, we have performed repeated simulations at different volumes and spacings $a \propto \beta_G^{-1}$, and verified that the transition remains first order as $V \to \infty, a \to 0$. For the critical temperature T_c, volume dependence is found to be extremely mild, but there is linear dependence on β_G^{-1}. The extrapolation $a \to 0$ is shown in panel (b) on fig. 7.1. Statistical errors are extremely small, as shown by the error bars.

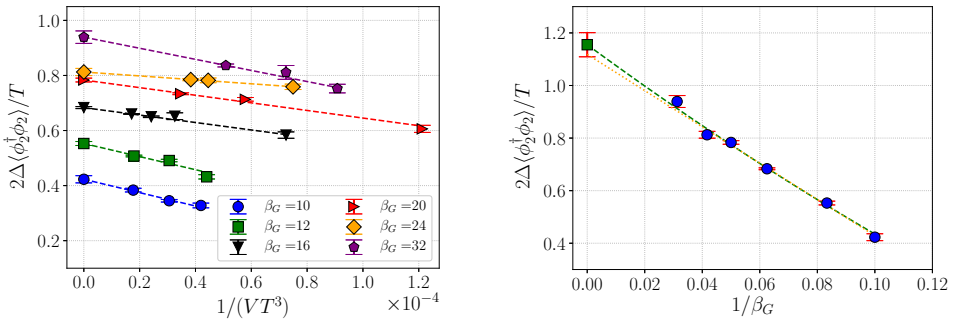

(a) (b)

Figure 7.2: Extrapolations of the $\phi_2^\dagger\phi_2$ condensate discontinuity to infinite volume (left) and to continuum (right). The right-hand plot uses the $V \to \infty$ extrapolations and shows both linear (dotted) and quadratic (dashed) fits, which agree within statistical errors.

In contrast, the EWPT strength in this benchmark point is sensitive to the volume and exhibits strong lattice spacing dependence. This is depicted for the $\langle\phi_2^\dagger\phi_2\rangle$ discontinuity in fig. 7.2. Panel (a) shows volume dependence and $V \to \infty$ extrapolations at different lattice spacings, and the continuum extrapolation is shown in panel (b). The behavior of $\langle\phi_1^\dagger\phi_1\rangle$ is similar, but its discontinuity is much smaller. We observe that the $\langle\phi_2^\dagger\phi_2\rangle$ discontinuity varies by over a factor of two between the coarsest and finest lattices. The dependence on a is larger than in the MSSM study of [155] and substantially more severe than in the SU(2)+ Higgs theory [85]. This may hint at the presence of heavy BSM excitations that become fully dynamical only at small a. Another source of a-dependence arises from our lattice-continuum relations, which are exact up to perturbative $O(a)$ corrections [155]. But in this case our largest coupling is, at zero temperature, $\lambda_3 \approx 2.7$, which is much larger than couplings in the MSSM. Therefore, enhanced sensitivity to the missing $O(a)$ terms is to be expected.

The above discussion demonstrates that lattice-spacing effects can be a serious source of uncertainty in BSM theories. This is not a fundamental obstacle for non-perturbative studies, but can increase the numerical cost of simulations as more lattice sites are needed at small a to properly capture the IR dynamics. Our results in the 2HDM indicate that finite-volume effects are mostly overshadowed by the sensitivity to a, and this is true also for the latent heat and surface tension, for which extrapolations can be found in [1]. We also repeated the lattice analysis for an another set of 2HDM parameters with slightly stronger EWPT, where finite-size effects of the same magnitude were found.

It is interesting to compare the non-perturbative results to those obtained with perturbative methods. The numbers for $T_c, v/T_c$[26] and latent heat L in two benchmark points are listed in ta-

[26]The lattice value for $\Delta v/T$ refers to $\sqrt{2\Delta\langle\phi_2^\dagger\phi_2\rangle/T}$ while the perturbative quantity is the jump of $v/T = \sqrt{v_1^2 + v_2^2}/T$ in R_ξ Landau gauge, where v_1 and v_2 are VEVs of the neutral scalar components of ϕ_1 and ϕ_2 rescaled to 4d units. On the lattice there is also a small jump in $\langle\phi_1^\dagger\phi_1\rangle$, which we neglect here.

	Method	T_c/GeV	L/T_c^4	$\Delta v/T_c$	L/GeV^4
BM1	1-loop Parwani resum.	134.0 ± 8.75	0.396 ± 0.002	1.01 ± 0.06	1.27×10^8
	1-loop A-E resum.	142.4 ± 6.88	0.33 ± 0.02	1.00 ± 0.07	1.37×10^8
	2-loop in 3d	111.6 ± 2.30	0.57 ± 0.10	0.98 ± 0.09	0.89×10^8
	3d lattice	116.40 ± 0.005	0.60 ± 0.02	1.08 ± 0.02	1.11×10^8
BM2	1-loop Parwani resum.	142.6 ± 18.0	0.29 ± 0.04	0.91 ± 0.06	1.19×10^8
	1-loop A-E resum.	162.5 ± 21.0	0.20 ± 0.03	0.88 ± 0.05	1.36×10^8
	2-loop in 3d	104.9 ± 2.30	0.61 ± 0.10	0.97 ± 0.06	0.74×10^8
	3d lattice	112.5 ± 0.01	0.81 ± 0.05	1.09 ± 0.03	1.29×10^8

Table 7.1: Comparison of perturbative and non-perturbative results in two 2HDM benchmark points admitting a first-order EWPT. The 1-loop calculations differ by the choice of resummation prescription as described in the text. Error bars for the perturbative results are obtained by varying the RG scale. Input parameters for the benchmark points are given in [1].

ble 7.1. We give 1-loop predictions using two different resummation prescriptions that appear frequently in the literature. First is the "Parwani" method which adds thermal masses to all Matsubara modes [152], whereas the second "Arnold-Espinosa" (A-E) method resums only zero-mode propagators [134] and is thus equivalent to the 3d approach. In the high-T limit, the difference between the 1-loop calculations is formally of 2-loop order. Error bars in perturbative results correspond to residual RG-scale sensitivity as described in the paper [1], and for lattice results we show the statistical errors. For brevity, only the central value is shown for L.

The 1-loop potentials are seen to seriously overestimate the critical temperature, resulting in too small values for L/T_c^4. 2-loop results in contrast are within $\sim 10\%$ of the non-perturbative values, suggesting that the 2-loop potential should be reasonably accurate at least for the equilibrium quantities T_c and L/T_c^4 in the 2HDM, when the EWPT is strongly first order. Thus there are prospects for improved graviational-wave and baryogenesis studies at the 2-loop level, at least until lattice results in broader regions of the free parameter space become available.

7.3 Two-step electroweak phase transition on the lattice

In chapter 5 we mentioned that in BSM theories the EWPT can occur in two stages. The first step at $T > T_{\rm EW}$ is the transition into a phase characterized by non-zero VEV of some BSM field, and as the universe cools down, the usual Higgs mechanism takes place at $T_{\rm EW}$ and the theory ends up in the standard EW vacuum. If the BSM field is charged under the EW symmetry, the theory then undergoes a two-step Higgs mechanism where the EW symmetry is "spontaneously broken" already in the intermediate phase.[27] This scenario is motivated by prospects for baryogenesis, as the baryon asymmetry could be generated already during the first transition, but also because the second transition would naturally occur through a tree-level saddle point and could

[27]The discussion of section 4.1 naturally applies here as well: the different "phases" may actually be analytically connected.

be very strongly first order, and thus favorable for gravitational-wave production. Cosmological consequences of two-step EWPTs have been investigated perturbatively in different models [46, 53, 54, 62, 63, 74]. In paper [2], we studied two-step EWPTs non-perturbatively in a triplet-extended model (the "ΣSM").

The model in question is defined by the Lagrangian

$$\mathcal{L} = \mathcal{L}_{\mathrm{SM}} + \frac{1}{2}(D_\mu \Sigma^a)^2 + \frac{1}{2} m_\Sigma^2 \Sigma^a \Sigma^a + \frac{1}{4} b_4 (\Sigma^a \Sigma^a)^2 + \frac{1}{2} a_2 \phi^\dagger \phi \Sigma^a \Sigma^a, \tag{7.4}$$

where Σ^a are components of a real-valued SU(2) triplet, $\Sigma = \frac{1}{2}\Sigma^a \sigma^a$. In other words, Σ is an adjoint scalar field. The covariant derivative is $D_\mu \Sigma^a = \partial_\mu \Sigma^a - ig\epsilon_{abc} A_\mu^b \Sigma^c$. This form of the scalar potential is symmetric under the Z_2 transformation $\Sigma \to -\Sigma$, which ensures that the model is consistent with experimental bounds on the EW ρ parameter [182]. There are three BSM excitations with degenerate masses at tree level; in the following we denote the electrically-neutral component mass by M_Σ. Phenomenological studies of the model at $T = 0$ appear in [182–184].

Two-step EWPTs in the triplet model were studied first at 1-loop level in [53]. The calculations are straightforwardly extended to 2-loop level using dimensional reduction, which was carried out in [96]. Lattice simulations were performed in [2]. Neglecting again the hypercharge interaction, the dimensionally-reduced theory in lattice discretization is

$$\begin{aligned} S_{\Sigma\mathrm{SM}}^{(3\mathrm{d})} = S_W &+ 2a \sum_{x,i} \left[\phi^\dagger \phi - \mathrm{Re}\, \phi^\dagger(x) U_i(x) \phi(x+i) + \mathrm{Tr}\, \Sigma^2 - \mathrm{Tr}\, \Sigma(x) U_i(x) \Sigma(x+i) U_i^\dagger(x) \right] \\ &+ a^3 \sum_x \left[\bar{m}_\phi^2 \phi^\dagger \phi + \bar{m}_\Sigma^2 \,\mathrm{Tr}\, \Sigma^2 + \bar{\lambda} (\phi^\dagger \phi)^2 + \bar{b}_4 \left(\mathrm{Tr}\, \Sigma^2 \right)^2 + \bar{a}_2 \phi^\dagger \phi \,\mathrm{Tr}\, \Sigma^2 \right]. \end{aligned} \tag{7.5}$$

The relevant lattice-continuum relations can be read from [171].

Two-step EWPT occurs if the triplet field condenses at a higher temperature than the Higgs doublet. As a first approximation, we may scan the parameter space for two-step transitions using the perturbative effective potential. The scans reveal a narrow band in (M_Σ, a_2) plane where two-step transitions are realized, in agreement with the 1-loop study of [53]. This is shown in fig. 7.3, which combines also results of [2] to distinguish between direct one-step first-order and crossover transitions. The two-step EWPT is, in some sense, a rather rare occurrence, as the majority of the allowed parameter space has only direct transitions into the EW Higgs regime. The two-step scenario is constrained by the requirement that the EW vacuum should be the global minimum of the $T = 0$ potential, and this is not satisfied in most of the parameter space where Σ can condense.[28] Nevertheless, it is interesting to consider two-step EWPTs also in non-perturbative detail.

The crosses in fig. 7.3 show points where we have carried out lattice simulations in the EFT (7.5). Two-step EWPT are indeed found in the narrow band predicted by 2-loop perturbation theory, but the nature of these transitions can differ drastically from perturbative predictions. The intermediate phase where Σ is condensed admits a *perturbatively* massless photon-like excitation, corresponding to a residual U(1) symmetry. However, at the non-perturbative level this phase contains 't Hooft-Polyakov magnetic monopoles [185, 186], and the photon is replaced by

[28] Further constraints come from real-time considerations of bubble nucleations in the expanding universe and are not considered here.

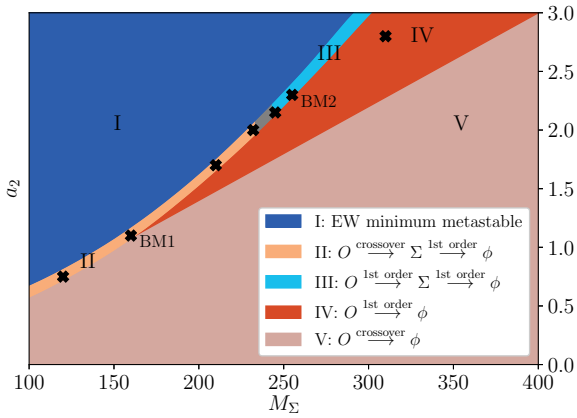

Figure 7.3: Phase diagram for the triplet model at fixed $b_4 = 0.25$. Regions II-V correspond to different types of phase transitions starting from the symmetric phase O and ending in the EW Higgs phase. In regions II and III there exists an intermediate phase where the triplet field condenses. The $O \to \Sigma$ phase transition terminates somewhere in the gray region, and in region II this transition is a smooth crossover. In region I the EW vacuum is not the global minimum of the $T = 0$ effective potential. The crosses indicate non-perturbative lattice benchmark points.

a massive pseudoscalar excitation. Consequently, the Σ phase is actually analytically connected to the symmetric phase, so that the first transition may be a crossover [107].

For small M_Σ and a_2, we indeed we find crossovers in the first step. This is demonstrated in fig. 7.4, which plots the dimensionless susceptibility of $\mathrm{Tr}\,\Sigma^2$ in one point (BM1 in fig. 7.3), specifically

$$\chi(\Sigma^2) = VT\left[\langle(\mathrm{Tr}\,\Sigma^2)_V^2\rangle - \langle(\mathrm{Tr}\,\Sigma^2)_V\rangle^2\right], \tag{7.6}$$

where the subscript denotes volume averaging. This susceptibility is discontinuous in first-order transitions, and diverges with a critical exponent as $V \to \infty$ if the transition is second order. According to fig. 7.4, the peak susceptibility converges to a finite value at large volumes, consistent with crossover behavior. The symmetric $\to \Sigma$ transitions are crossovers in region II of fig. 7.3, but turn into first-order transitions in region III. There is a line of second-order transitions somewhere in the gray region between II and III, but we have not attempted a more precise determination of this end line. A two-step baryogenesis scenario as sketched in [53] necessitates a first-order phase transition in the Σ direction and is thus ruled out in region II. In contrast, the second transition between Σ and ϕ regimes is found to always be first order, in agreement with perturbative expectations.

In the previous section we found that the lattice results can contain severe $O(a)$ errors, presumably because the scalar potential contains relatively large couplings. We have performed a similar investigation of lattice artifacts also in the triplet-extended model, and some extrapolations are shown in fig. 7.5. The data is for the $\Sigma \to \phi$ transition in point BM2 of fig. 7.3, which is

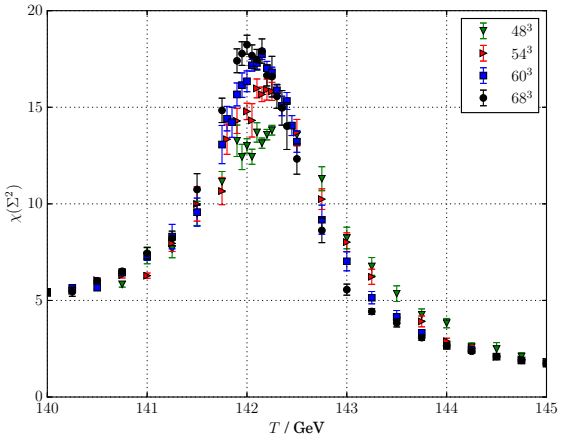

Figure 7.4: The susceptibility of eq. (7.6) plotted at different volumes on a $\beta_G = 24$ lattice. The large-volume behavior is consistent with crossover behavior in the symmetric $\longrightarrow \Sigma$ step.

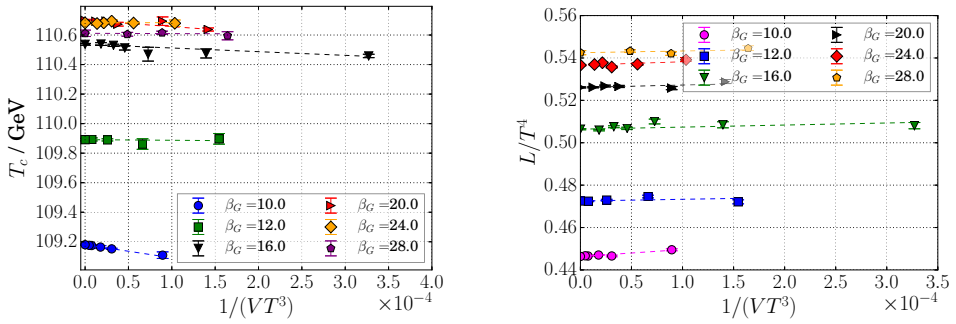

(a) (b)

Figure 7.5: Infinite volume extrapolations for the latter transition in point BM2 at different lattice spacings.

strongly first order. The critical temperature in panel (a) is fairly insensitive both to β_G and the volume, while the latent heat in panel (b) shows considerable sensitivity to the lattice spacing. However, overall the discretization errors are milder than in the 2HDM benchmarks and satisfactory convergence to the continuum result is seen for $\beta_G \gtrsim 20$. We do not show separate plots for $a \longrightarrow 0$ extrapolations.

Let us conclude with a comparison to perturbative results. Fig. 7.6 shows the evolution of quadratic scalar condensates in points BM1 and BM2, together with 2-loop estimates. The intermediate Σ phase is clearly visible in both points. The perturbative curves have been obtained

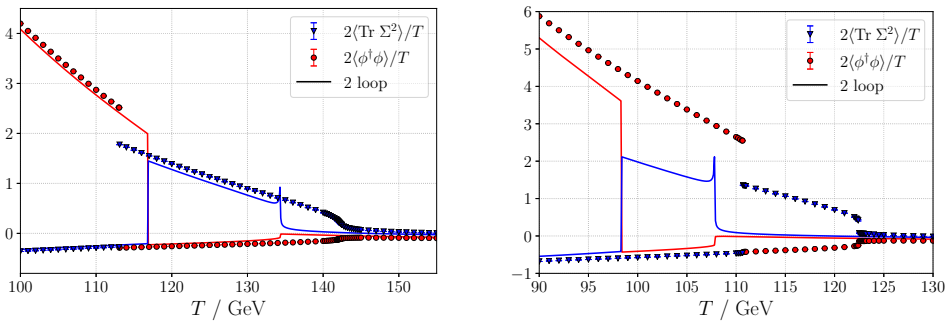

(a) BM1

(b) BM2

Figure 7.6: Higgs and triplet condensates as obtained from lattice simulations ($\beta_G = 24, V = 60^3$) and from 2-loop effective potential (solid lines). The condensates are scheme dependent and given in here in the $\overline{\mathrm{MS}}$ scheme. The relations for converting between lattice and $\overline{\mathrm{MS}}$ condensates are given in [171].

using the gauge-invariant approach of [148], which unfortunately fails near the first transition because of an explicit IR divergence at 2-loop level [147]. This is visible as the "spikes" in the Σ^2 condensate near T_c. Apart from this issue, 2-loop perturbation theory is seen to deviate by $\sim 10\%$ in its predictions for the critical temperatures, and the condensate jumps are slightly underestimated. The quantity L/T^4 differs by $30\% - 40\%$ from the lattice results. Thus the non-perturbative approach seems necessary also for two-step EWPT if the strength needs to be known at better than 40% accuracy.

Frequently in the literature, it is assumed that loop corrections should be small or even negligible for the second transition into the ϕ phase, because the potential barrier is present already in the tree-level potential. This is overly optimistic, as is obvious from our results. The reason is easily understood based already on the discussion of section 5.5. The expansion parameter associated with scalar loops is parametrically $a_2 T/m$, where m is the lightest field appearing in the loops. Because a_2 is large, the scalars would need to be relatively heavy for this ratio to be small. Indeed, numerically computing the thermal masses near the second transition and accounting also for the contribution from background fields, we find that the expansion parameter is > 1. Thus there is no *a priori* reason to believe that a low-order perturbative result would be even qualitatively correct.

Chapter 8

Summary and outlook

The study of finite-T phase transitions in particle physics models is an exciting topic, not least for the cosmological implications associated with possible first-order transitions in the early universe. This thesis has discussed phase transitions in the Higgs sector and the methodology required to rigorously establish both the existence and basic thermodynamics of such transitions from first principles. We have described the absence of an electroweak phase transition of any order in the Standard Model, and argued that already minimal modifications to the Higgs potential can catalyze a first-order transition in the electroweak sector. The fundamentally non-perturbative nature of these transitions has been emphasized, and as a solution we advocated a combination of finite-T perturbation theory for the weakly-coupled field modes, and lattice Monte Carlo simulations for the non-perturbative long-wavelength excitations.

The non-perturbative approach was applied to a selection of well-motivated theories beyond the Standard Model to build a robust understanding of the phase transition in these models. Although the required numerical effort forced us to mostly concentrate the analysis on selected benchmark points, we believe the results to be valuable both as a non-perturbative confirmation that the models can exhibit a strongly first-order electroweak phase transition, but also as a testing ground for other, less reliable methods of computation. In particular, we consistently found considerable deviations from 2-loop perturbative predictions in both v/T and the critical temperature. We demonstrated that this error amounts to uncertainty of several tens of percents in the transition strength as measured by the latent heat, L/T^4. This uncertainty propagates in particular to predictions of gravitational-wave spectra, which are notoriously sensitive to the underlying thermodynamical parameters [83, 84]. We therefore anticipate that non-perturbative determination of these quantities will be necessary for solid estimates related to gravitational waves, and possibly for baryogenesis calculations as well.

Most existing studies of the electroweak phase transition and associated cosmological applications work only at the 1-loop level [46–79], even though the 2-loop improvement has been shown to be very significant [1, 3, 82]. While inferior to a proper non-perturbative treatment, the 2-loop potential is numerically much more manageable than large-scale Monte Carlo simulations. Based on the results of [1, 3], one may even hope to obtain T_c and v/T_c within $\sim 10\%$ of the non-perturbative value using the 2-loop effective potential. With these observations, we believe there are strong motivations to extend past investigations of the phase transition in theories beyond

the Standard Model to at least the 2-loop level.

Besides the equilibrium parameters $T_c, v/T, L/T^4$, for physical applications it is necessary to study also the real-time dynamics of the transition. Looking ahead, the next logical step is to apply the non-perturbative techniques to study the bubble nucleation rate. In fact, the framework of dimensionally-reduced theories is appropriate also for this quantity [140]. Given that the nucleation rate is poorly understood even in the analytical approximation [84], we expect the non-perturbative methodology described in this thesis to play a major role also in future studies of cosmological phase transitions.

Bibliography

[1] K. Kainulainen, V. Keus, L. Niemi, K. Rummukainen, T. V. I. Tenkanen, and V. Vaskonen, JHEP **06**, 075 (2019), arXiv:1904.01329 [hep-ph] .

[2] L. Niemi, M. Ramsey-Musolf, T. V. I. Tenkanen, and D. J. Weir, Phys. Rev. Lett. **126**, 171802 (2021), arXiv:2005.11332 [hep-ph] .

[3] L. Niemi, P. Schicho, and T. V. I. Tenkanen, Phys. Rev. D **103**, 115035 (2021), arXiv:2103.07467 [hep-ph] .

[4] G. Aad *et al.* (ATLAS), Phys. Lett. B **716**, 1 (2012), arXiv:1207.7214 [hep-ex] .

[5] S. Chatrchyan *et al.* (CMS), Phys. Lett. B **716**, 30 (2012), arXiv:1207.7235 [hep-ex] .

[6] Y. Aoki, G. Endrodi, Z. Fodor, S. D. Katz, and K. K. Szabo, Nature **443**, 675 (2006), arXiv:hep-lat/0611014 .

[7] K. Kajantie, M. Laine, K. Rummukainen, and M. E. Shaposhnikov, Phys. Rev. Lett. **77**, 2887 (1996), arXiv:hep-ph/9605288 [hep-ph] .

[8] F. Csikor, Z. Fodor, and J. Heitger, Phys. Rev. Lett. **82**, 21 (1999), arXiv:hep-ph/9809291 [hep-ph] .

[9] M. A. Stephanov, PoS **LAT2006**, 024 (2006), arXiv:hep-lat/0701002 .

[10] V. A. Kuzmin, V. A. Rubakov, and M. E. Shaposhnikov, Phys. Lett. **155B**, 36 (1985).

[11] M. E. Shaposhnikov, JETP Lett. **44**, 465 (1986), [Pisma Zh. Eksp. Teor. Fiz.44,364(1986)].

[12] M. E. Shaposhnikov, Nucl. Phys. **B287**, 757 (1987).

[13] P. A. R. Ade *et al.* (Planck), Astron. Astrophys. **594**, A13 (2016), arXiv:1502.01589 [astro-ph.CO] .

[14] A. D. Sakharov, Pisma Zh. Eksp. Teor. Fiz. **5**, 32 (1967).

[15] S. L. Adler, Phys. Rev. **177**, 2426 (1969).

[16] M. E. Shaposhnikov, Nucl. Phys. B **299**, 797 (1988).

[17] M. B. Gavela, P. Hernandez, J. Orloff, and O. Pene, Mod. Phys. Lett. A **9**, 795 (1994), arXiv:hep-ph/9312215 .

[18] P. Huet and E. Sather, Phys. Rev. D **51**, 379 (1995), arXiv:hep-ph/9404302 .

[19] M. B. Gavela, P. Hernandez, J. Orloff, O. Pene, and C. Quimbay, Nucl. Phys. B **430**, 382 (1994), arXiv:hep-ph/9406289 .

[20] A. G. Cohen, D. B. Kaplan, and A. E. Nelson, Ann. Rev. Nucl. Part. Sci. **43**, 27 (1993), arXiv:hep-ph/9302210 .

[21] J. M. Cline, in *Les Houches Summer School - Session 86: Particle Physics and Cosmology: The Fabric of Spacetime* (2006) arXiv:hep-ph/0609145 .

[22] D. E. Morrissey and M. J. Ramsey-Musolf, New J. Phys. **14**, 125003 (2012), arXiv:1206.2942 [hep-ph] .

[23] E. Witten, Phys. Rev. D **30**, 272 (1984).

[24] C. J. Hogan, Mon. Not. Roy. Astron. Soc. **218**, 629 (1986).

[25] A. Kosowsky, M. S. Turner, and R. Watkins, Phys. Rev. D **45**, 4514 (1992).

[26] A. Kosowsky, M. S. Turner, and R. Watkins, Phys. Rev. Lett. **69**, 2026 (1992).

[27] M. Hindmarsh, S. J. Huber, K. Rummukainen, and D. J. Weir, Phys. Rev. Lett. **112**, 041301 (2014), arXiv:1304.2433 [hep-ph] .

[28] J. T. Giblin and J. B. Mertens, Phys. Rev. D **90**, 023532 (2014), arXiv:1405.4005 [astro-ph.CO] .

[29] M. Hindmarsh, S. J. Huber, K. Rummukainen, and D. J. Weir, Phys. Rev. D **92**, 123009 (2015), arXiv:1504.03291 [astro-ph.CO] .

[30] M. Hindmarsh, S. J. Huber, K. Rummukainen, and D. J. Weir, Phys. Rev. D **96**, 103520 (2017), [Erratum: Phys.Rev.D 101, 089902 (2020)], arXiv:1704.05871 [astro-ph.CO] .

[31] C. Caprini *et al.*, JCAP **04**, 001 (2016), arXiv:1512.06239 [astro-ph.CO] .

[32] C. Caprini *et al.*, JCAP **03**, 024 (2020), arXiv:1910.13125 [astro-ph.CO] .

[33] G. M. Harry, P. Fritschel, D. A. Shaddock, W. Folkner, and E. S. Phinney, Class. Quant. Grav. **23**, 4887 (2006), [Erratum: Class.Quant.Grav. 23, 7361 (2006)].

[34] S. Kawamura *et al.*, Class. Quant. Grav. **28**, 094011 (2011).

[35] W.-H. Ruan, Z.-K. Guo, R.-G. Cai, and Y.-Z. Zhang, Int. J. Mod. Phys. A **35**, 2050075 (2020), arXiv:1807.09495 [gr-qc] .

[36] J. R. Espinosa, T. Konstandin, J. M. No, and G. Servant, JCAP **06**, 028 (2010), arXiv:1004.4187 [hep-ph] .

[37] M. J. Ramsey-Musolf, JHEP **09**, 179 (2020), arXiv:1912.07189 [hep-ph] .

[38] J. Kozaczuk, M. J. Ramsey-Musolf, and J. Shelton, Phys. Rev. D **101**, 115035 (2020), arXiv:1911.10210 [hep-ph] .

[39] H. Baer *et al.*, (2013), arXiv:1306.6352 [hep-ph] .

[40] M. Dong *et al.* (CEPC Study Group), (2018), arXiv:1811.10545 [hep-ex] .

[41] R. Franceschini *et al.*, **3/2018** (2018), 10.23731/CYRM-2018-003, arXiv:1812.02093 [hep-ph] .

[42] A. Abada *et al.* (FCC), Eur. Phys. J. C **79**, 474 (2019).

[43] C. Caprini and D. G. Figueroa, Class. Quant. Grav. **35**, 163001 (2018), arXiv:1801.04268 [astro-ph.CO] .

[44] A. D. Linde, Phys. Lett. **96B**, 289 (1980).

[45] D. J. Gross, R. D. Pisarski, and L. G. Yaffe, Rev. Mod. Phys. **53**, 43 (1981).

[46] A. Hammerschmitt, J. Kripfganz, and M. G. Schmidt, Z. Phys. C **64**, 105 (1994), arXiv:hep-ph/9404272 .

[47] J. M. Cline and P.-A. Lemieux, Phys. Rev. D **55**, 3873 (1997), arXiv:hep-ph/9609240 .

[48] L. Fromme, S. J. Huber, and M. Seniuch, JHEP **11**, 038 (2006), arXiv:hep-ph/0605242 .

[49] S. Profumo, M. J. Ramsey-Musolf, and G. Shaughnessy, JHEP **08**, 010 (2007), arXiv:0705.2425 [hep-ph] .

[50] A. Ashoorioon and T. Konstandin, JHEP **07**, 086 (2009), arXiv:0904.0353 [hep-ph] .

[51] J. R. Espinosa, T. Konstandin, and F. Riva, Nucl. Phys. B **854**, 592 (2012), arXiv:1107.5441 [hep-ph] .

[52] J. M. Cline, K. Kainulainen, and M. Trott, JHEP **11**, 089 (2011), arXiv:1107.3559 [hep-ph] .

[53] H. H. Patel and M. J. Ramsey-Musolf, Phys. Rev. D **88**, 035013 (2013), arXiv:1212.5652 [hep-ph] .

[54] H. H. Patel, M. J. Ramsey-Musolf, and M. B. Wise, Phys. Rev. D **88**, 015003 (2013), arXiv:1303.1140 [hep-ph] .

[55] G. C. Dorsch, S. J. Huber, and J. M. No, JHEP **10**, 029 (2013), arXiv:1305.6610 [hep-ph] .

[56] S. Profumo, M. J. Ramsey-Musolf, C. L. Wainwright, and P. Winslow, Phys. Rev. D **91**, 035018 (2015), arXiv:1407.5342 [hep-ph] .

[57] D. Curtin, P. Meade, and C.-T. Yu, JHEP **11**, 127 (2014), arXiv:1409.0005 [hep-ph] .

[58] G. C. Dorsch, S. J. Huber, K. Mimasu, and J. M. No, Phys. Rev. Lett. **113**, 211802 (2014), arXiv:1405.5537 [hep-ph] .

[59] K. Fuyuto and E. Senaha, Phys. Rev. D **90**, 015015 (2014), arXiv:1406.0433 [hep-ph] .

[60] J. Kozaczuk, JHEP **10**, 135 (2015), arXiv:1506.04741 [hep-ph] .

[61] N. Blinov, S. Profumo, and T. Stefaniak, JCAP **07**, 028 (2015), arXiv:1504.05949 [hep-ph] .

[62] N. Blinov, J. Kozaczuk, D. E. Morrissey, and C. Tamarit, Phys. Rev. D **92**, 035012 (2015), arXiv:1504.05195 [hep-ph] .

[63] S. Inoue, G. Ovanesyan, and M. J. Ramsey-Musolf, Phys. Rev. D **93**, 015013 (2016), arXiv:1508.05404 [hep-ph] .

[64] G. C. Dorsch, S. J. Huber, T. Konstandin, and J. M. No, JCAP **05**, 052 (2017), arXiv:1611.05874 [hep-ph] .

[65] P. Basler, M. Krause, M. Muhlleitner, J. Wittbrodt, and A. Wlotzka, JHEP **02**, 121 (2017), arXiv:1612.04086 [hep-ph] .

[66] C.-W. Chiang, K. Fuyuto, and E. Senaha, Phys. Lett. B **762**, 315 (2016), arXiv:1607.07316 [hep-ph] .

[67] M. Chala, G. Nardini, and I. Sobolev, Phys. Rev. D **94**, 055006 (2016), arXiv:1605.08663 [hep-ph] .

[68] V. Vaskonen, Phys. Rev. D **95**, 123515 (2017), arXiv:1611.02073 [hep-ph] .

[69] A. Beniwal, M. Lewicki, J. D. Wells, M. White, and A. G. Williams, JHEP **08**, 108 (2017), arXiv:1702.06124 [hep-ph] .

[70] G. Kurup and M. Perelstein, Phys. Rev. **D96**, 015036 (2017), arXiv:1704.03381 [hep-ph] .

[71] C.-Y. Chen, J. Kozaczuk, and I. M. Lewis, JHEP **08**, 096 (2017), arXiv:1704.05844 [hep-ph] .

[72] P. Basler, M. Mühlleitner, and J. Wittbrodt, JHEP **03**, 061 (2018), arXiv:1711.04097 [hep-ph] .

[73] K. Fuyuto, W.-S. Hou, and E. Senaha, Phys. Lett. B **776**, 402 (2018), arXiv:1705.05034 [hep-ph] .

[74] M. J. Ramsey-Musolf, P. Winslow, and G. White, Phys. Rev. D **97**, 123509 (2018), arXiv:1708.07511 [hep-ph] .

[75] C.-W. Chiang, Y.-T. Li, and E. Senaha, Phys. Lett. B **789**, 154 (2019), arXiv:1808.01098 [hep-ph] .

[76] M. Carena, Z. Liu, and Y. Wang, JHEP **08**, 107 (2020), arXiv:1911.10206 [hep-ph] .

[77] A. Papaefstathiou and G. White, JHEP **05**, 099 (2021), arXiv:2010.00597 [hep-ph] .

[78] P. Basler, M. Mühlleitner, and J. Müller, JHEP **05**, 016 (2020), arXiv:1912.10477 [hep-ph] .

[79] W. Su, A. G. Williams, and M. Zhang, JHEP **04**, 219 (2021), arXiv:2011.04540 [hep-ph] .

[80] D. Bodeker, P. John, M. Laine, and M. G. Schmidt, Nucl. Phys. B **497**, 387 (1997), arXiv:hep-ph/9612364 .

[81] M. Laine, G. Nardini, and K. Rummukainen, JCAP **01**, 011 (2013), arXiv:1211.7344 [hep-ph] .

[82] M. Laine, M. Meyer, and G. Nardini, Nucl. Phys. **B920**, 565 (2017), arXiv:1702.07479 [hep-ph] .

[83] D. Croon, O. Gould, P. Schicho, T. V. I. Tenkanen, and G. White, JHEP **04**, 055 (2021), arXiv:2009.10080 [hep-ph] .

[84] O. Gould and T. V. I. Tenkanen, JHEP **06**, 069 (2021), arXiv:2104.04399 [hep-ph] .

[85] K. Kajantie, M. Laine, K. Rummukainen, and M. E. Shaposhnikov, Nucl. Phys. **B466**, 189 (1996), arXiv:hep-lat/9510020 [hep-lat] .

[86] K. Kajantie, M. Laine, K. Rummukainen, and M. E. Shaposhnikov, Nucl. Phys. **B493**, 413 (1997), arXiv:hep-lat/9612006 [hep-lat] .

[87] M. Gurtler, E.-M. Ilgenfritz, and A. Schiller, Phys. Rev. D **56**, 3888 (1997), arXiv:hep-lat/9704013 .

[88] M. D'Onofrio and K. Rummukainen, Phys. Rev. D **93**, 025003 (2016), arXiv:1508.07161 [hep-ph] .

[89] P. H. Ginsparg, Nucl. Phys. **B170**, 388 (1980).

[90] T. Appelquist and R. D. Pisarski, Phys. Rev. **D23**, 2305 (1981).

[91] K. Farakos, K. Kajantie, K. Rummukainen, and M. E. Shaposhnikov, Nucl. Phys. **B425**, 67 (1994), arXiv:hep-ph/9404201 [hep-ph] .

[92] K. Farakos, K. Kajantie, K. Rummukainen, and M. E. Shaposhnikov, Nucl. Phys. **B442**, 317 (1995), arXiv:hep-lat/9412091 [hep-lat] .

[93] K. Kajantie, M. Laine, K. Rummukainen, and M. E. Shaposhnikov, Nucl. Phys. **B458**, 90 (1996), arXiv:hep-ph/9508379 [hep-ph] .

[94] J. O. Andersen, T. Gorda, A. Helset, L. Niemi, T. V. I. Tenkanen, A. Tranberg, A. Vuorinen, and D. J. Weir, Phys. Rev. Lett. **121**, 191802 (2018), arXiv:1711.09849 [hep-ph] .

[95] T. Gorda, A. Helset, L. Niemi, T. V. I. Tenkanen, and D. J. Weir, JHEP **02**, 081 (2019), arXiv:1802.05056 [hep-ph] .

[96] L. Niemi, H. H. Patel, M. J. Ramsey-Musolf, T. V. I. Tenkanen, and D. J. Weir, Phys. Rev. D **100**, 035002 (2019), arXiv:1802.10500 [hep-ph] .

[97] O. Gould, J. Kozaczuk, L. Niemi, M. J. Ramsey-Musolf, T. V. I. Tenkanen, and D. J. Weir, Phys. Rev. D **100**, 115024 (2019), arXiv:1903.11604 [hep-ph] .

[98] J. I. Kapusta, *Finite Temperature Field Theory*, Cambridge Monographs on Mathematical Physics (Cambridge University Press, Cambridge, 1989).

[99] M. Laine and A. Vuorinen, *Basics of Thermal Field Theory*, Vol. 925 (Springer, 2016) arXiv:1701.01554 [hep-ph] .

[100] E. Braaten and A. Nieto, Phys. Rev. **D51**, 6990 (1995), arXiv:hep-ph/9501375 [hep-ph] .

[101] O. Gould, JHEP **04**, 057 (2021), arXiv:2101.05528 [hep-ph] .

[102] P. M. Schicho, T. V. I. Tenkanen, and J. Österman, JHEP **06**, 130 (2021), arXiv:2102.11145 [hep-ph] .

[103] N. P. Landsman, Nucl. Phys. B **322**, 498 (1989).

[104] S. Elitzur, Phys. Rev. D **12**, 3978 (1975).

[105] J. Greensite, Prog. Part. Nucl. Phys. **51**, 1 (2003), arXiv:hep-lat/0301023 .

[106] A. I. Bochkarev, S. Y. Khlebnikov, and M. E. Shaposhnikov, Nucl. Phys. B **329**, 493 (1990).

[107] K. Kajantie, M. Laine, K. Rummukainen, and M. E. Shaposhnikov, Nucl. Phys. B **503**, 357 (1997), arXiv:hep-ph/9704416 .

[108] K. Kajantie, M. Laine, K. Rummukainen, and M. E. Shaposhnikov, Phys. Lett. B **423**, 137 (1998), arXiv:hep-ph/9710538 .

[109] J. I. Kapusta, Nucl. Phys. B **148**, 461 (1979).

[110] P. B. Arnold and L. G. Yaffe, Phys. Rev. D **52**, 7208 (1995), arXiv:hep-ph/9508280 .

[111] M. Laine, P. Schicho, and Y. Schröder, Phys. Rev. D **101**, 023532 (2020), arXiv:1911.09123 [hep-ph] .

[112] J. Ghiglieri, A. Kurkela, M. Strickland, and A. Vuorinen, Phys. Rept. **880**, 1 (2020), arXiv:2002.10188 [hep-ph] .

[113] K. G. Wilson, Phys. Rev. D **10**, 2445 (1974).

[114] K. Symanzik, Nucl. Phys. B **226**, 187 (1983).

[115] H. J. Rothe, *Lattice gauge theories: An Introduction* (World Scientific Lecture Notes in Physics: Volume 43, 1992).

[116] V. N. Gribov, Nucl. Phys. B **139**, 1 (1978).

[117] I. M. Singer, Commun. Math. Phys. **60**, 7 (1978).

[118] M. Luscher, Subnucl. Ser. **38**, 41 (2002), arXiv:hep-th/0102028 .

[119] D. B. Kaplan, in *Les Houches Summer School: Session 93: Modern perspectives in lattice QCD: Quantum field theory and high performance computing* (2009) arXiv:0912.2560 [hep-lat] .

[120] D. M. Grabowska and D. B. Kaplan, Phys. Rev. Lett. **116**, 211602 (2016), arXiv:1511.03649 [hep-lat] .

[121] W. Caudy and J. Greensite, Phys. Rev. D **78**, 025018 (2008), arXiv:0712.0999 [hep-lat] .

[122] M. Creutz and T. N. Tudron, Phys. Rev. D **17**, 2619 (1978).

[123] K. Osterwalder and E. Seiler, Annals Phys. **110**, 440 (1978).

[124] E. H. Fradkin and S. H. Shenker, Phys. Rev. D **19**, 3682 (1979).

[125] A. Cherman, T. Jacobson, S. Sen, and L. G. Yaffe, Phys. Rev. D **102**, 105021 (2020), arXiv:2007.08539 [hep-th] .

[126] L. F. Abbott and E. Farhi, Phys. Lett. B **101**, 69 (1981).

[127] G. 't Hooft, NATO Sci. Ser. B **59**, 117 (1980).

[128] T. Banks and E. Rabinovici, Nucl. Phys. B **160**, 349 (1979).

[129] J. Frohlich, G. Morchio, and F. Strocchi, Phys. Lett. B **97**, 249 (1980).

[130] J. Frohlich, G. Morchio, and F. Strocchi, Nucl. Phys. B **190**, 553 (1981).

[131] A. Maas, Prog. Part. Nucl. Phys. **106**, 132 (2019), arXiv:1712.04721 [hep-ph] .

[132] Y. Aoki, Phys. Rev. D **56**, 3860 (1997), arXiv:hep-lat/9612023 .

[133] D. A. Kirzhnits and A. D. Linde, Annals Phys. **101**, 195 (1976).

[134] P. B. Arnold and O. Espinosa, Phys. Rev. **D47**, 3546 (1993), [Erratum: Phys. Rev.D50,6662(1994)], arXiv:hep-ph/9212235 [hep-ph] .

[135] Z. Fodor and A. Hebecker, Nucl. Phys. B **432**, 127 (1994), arXiv:hep-ph/9403219 .

[136] F. Karsch, T. Neuhaus, A. Patkos, and J. Rank, Nucl. Phys. B Proc. Suppl. **53**, 623 (1997), arXiv:hep-lat/9608087 .

[137] K. Rummukainen, M. Tsypin, K. Kajantie, M. Laine, and M. E. Shaposhnikov, Nucl. Phys. B **532**, 283 (1998), arXiv:hep-lat/9805013 .

[138] A. Gynther and M. Vepsalainen, JHEP **01**, 060 (2006), arXiv:hep-ph/0510375 .

[139] M. D'Onofrio, K. Rummukainen, and A. Tranberg, Phys. Rev. Lett. **113**, 141602 (2014), arXiv:1404.3565 [hep-ph] .

[140] G. D. Moore and K. Rummukainen, Phys. Rev. **D63**, 045002 (2001), arXiv:hep-ph/0009132 [hep-ph] .

[141] K. Assamagan *et al.* (2016) arXiv:1604.05324 [hep-ph] .

[142] O. Lebedev, Prog. Part. Nucl. Phys. **120**, 103881 (2021), arXiv:2104.03342 [hep-ph] .

[143] T. Robens and T. Stefaniak, Eur. Phys. J. C **75**, 104 (2015), arXiv:1501.02234 [hep-ph] .

[144] S. Adhikari, I. M. Lewis, and M. Sullivan, Phys. Rev. D **103**, 075027 (2021), arXiv:2003.10449 [hep-ph] .

[145] S. R. Coleman and E. J. Weinberg, Phys. Rev. D **7**, 1888 (1973).

[146] R. Jackiw, Phys. Rev. D **9**, 1686 (1974).

[147] M. Laine, Phys. Rev. **D51**, 4525 (1995), arXiv:hep-ph/9411252 [hep-ph] .

[148] H. H. Patel and M. J. Ramsey-Musolf, JHEP **07**, 029 (2011), arXiv:1101.4665 [hep-ph] .

[149] W. Buchmuller, Z. Fodor, and A. Hebecker, Phys. Lett. B **331**, 131 (1994), arXiv:hep-ph/9403391 .

[150] R. Fukuda and E. Kyriakopoulos, Nucl. Phys. B **85**, 354 (1975).

[151] M. Carrington, Phys. Rev. D **45**, 2933 (1992).

[152] R. R. Parwani, Phys. Rev. D **45**, 4695 (1992), [Erratum: Phys.Rev.D 48, 5965 (1993)], arXiv:hep-ph/9204216 .

[153] E. J. Weinberg and A.-q. Wu, Phys. Rev. D **36**, 2474 (1987).

[154] M. Laine and K. Rummukainen, Nucl. Phys. B **535**, 423 (1998), arXiv:hep-lat/9804019 .

[155] M. Laine and K. Rummukainen, Nucl. Phys. B **597**, 23 (2001), arXiv:hep-lat/0009025 .

[156] M. Creutz, *Quarks, gluons and lattices*, Cambridge Monographs on Mathematical Physics (Cambridge Univ. Press, Cambridge, UK, 1985).

[157] N. Madras and A. D. Sokal, J. Statist. Phys. **50**, 109 (1988).

[158] A. Sokal and L. Thomas, Journal of Statistical Physics **54**, 797 (1989).

[159] A. Sokal, "Monte carlo methods in statistical mechanics: Foundations and new algorithms," in *Functional Integration: Basics and Applications*, edited by C. DeWitt-Morette, P. Cartier, and A. Folacci (Springer US, Boston, MA, 1997) pp. 131–192.

[160] R. G. Miller, Biometrika **61**, 1 (1974).

[161] H. Flyvbjerg and H. G. Petersen, The Journal of Chemical Physics **91**, 461 (1989), https://doi.org/10.1063/1.457480 .

[162] N. Metropolis, A. W. Rosenbluth, M. N. Rosenbluth, A. H. Teller, and E. Teller, J. Chem. Phys. **21**, 1087 (1953).

[163] A. D. Kennedy and B. J. Pendleton, Phys. Lett. B **156**, 393 (1985).

[164] B. A. Berg and T. Neuhaus, Phys. Lett. B **267**, 249 (1991).

[165] B. A. Berg and T. Neuhaus, Phys. Rev. Lett. **68**, 9 (1992), arXiv:hep-lat/9202004 .

[166] F. Wang and D. P. Landau, Phys. Rev. Lett. **86**, 2050 (2001), arXiv:cond-mat/0011174 .

[167] A. M. Ferrenberg and R. H. Swendsen, Phys. Rev. Lett. **61**, 2635 (1988).

[168] A. D. Linde, Nucl. Phys. B **216**, 421 (1983), [Erratum: Nucl.Phys.B 223, 544 (1983)].

[169] K. Binder, Phys. Rev. A **25**, 1699 (1982).

[170] Y. Iwasaki, K. Kanaya, L. Karkkainen, K. Rummukainen, and T. Yoshie, Phys. Rev. D **49**, 3540 (1994), arXiv:hep-lat/9309003 .

[171] M. Laine, Nucl. Phys. B **451**, 484 (1995), arXiv:hep-lat/9504001 .

[172] M. Laine and A. Rajantie, Nucl. Phys. B **513**, 471 (1998), arXiv:hep-lat/9705003 .

[173] Z. Fodor, J. Hein, K. Jansen, A. Jaster, I. Montvay, and F. Csikor, Phys. Lett. B **334**, 405 (1994), arXiv:hep-lat/9405021 .

[174] Y. Aoki, F. Csikor, Z. Fodor, and A. Ukawa, Phys. Rev. D **60**, 013001 (1999), arXiv:hep-lat/9901021 .

[175] F. Csikor, Z. Fodor, P. Hegedus, A. Jakovac, S. D. Katz, and A. Piroth, Phys. Rev. Lett. **85**, 932 (2000), arXiv:hep-ph/0001087 .

[176] G. D. Moore, Nucl. Phys. B **493**, 439 (1997), arXiv:hep-lat/9610013 .

[177] G. D. Moore, Nucl. Phys. B **523**, 569 (1998), arXiv:hep-lat/9709053 .

[178] G. D. Moore and N. Schlusser, Phys. Rev. D **100**, 034510 (2019), arXiv:1905.09708 [hep-lat] .

[179] Y. Grossman, Nucl. Phys. B **426**, 355 (1994), arXiv:hep-ph/9401311 .

[180] G. C. Branco, P. M. Ferreira, L. Lavoura, M. N. Rebelo, M. Sher, and J. P. Silva, Phys. Rept. **516**, 1 (2012), arXiv:1106.0034 [hep-ph] .

[181] L. Altenkamp, S. Dittmaier, and H. Rzehak, JHEP **09**, 134 (2017), arXiv:1704.02645 [hep-ph] .

[182] P. Fileviez Perez, H. H. Patel, M. J. Ramsey-Musolf, and K. Wang, Phys. Rev. D **79**, 055024 (2009), arXiv:0811.3957 [hep-ph] .

[183] C.-W. Chiang, G. Cottin, Y. Du, K. Fuyuto, and M. J. Ramsey-Musolf, JHEP **01**, 198 (2021), arXiv:2003.07867 [hep-ph] .

[184] N. F. Bell, M. J. Dolan, L. S. Friedrich, M. J. Ramsey-Musolf, and R. R. Volkas, JHEP **05**, 050 (2020), arXiv:2001.05335 [hep-ph] .

[185] G. 't Hooft, Nucl. Phys. B **79**, 276 (1974).

[186] A. M. Polyakov, JETP Lett. **20**, 194 (1974).